ELSEVIER

Sedimentary Geology 92 (1994) 197–228

SEDIMENTARY GEOLOGY

The role of detrital composition and climate on the diagenetic evolution of continental molasses: evidence from the Cambro–Ordovician Guaritas Sequence, southern Brazil

Luiz F. De Ros [a,1], S. Morad [a], Paulo S.G. Paim [b,2]

[a] *Institute of Earth Sciences, Uppsala University, Norbyvägen 18B, S-752 36, Uppsala, Sweden*
[b] *University of Oxford, Earth Sciences Department, OX1 3PR, Oxford, UK*

Received October 14, 1993; revised version accepted March 17, 1994

Abstract

The Cambro–Ordovician molassic Guaritas Sequence (Camaquã Basin, southern Brazil) comprises alluvial-fan and braided fluvial sandstones and conglomerates with intercalated aeolian and lacustrine–deltaic deposits and andesitic lava flows. The sediments display a complex detrital composition derived from plutonic/gneissic, acidic volcanic and low-grade metamorphic source rocks. This detrital assemblage was strongly modified by semi-arid continental near-surface diagenesis. Early cementation by hematite, smectite, quartz and calcite, and the relatively limited burial prevented strong compaction and preserved some primary macroporosity in most of the sandstones, whereas the absence of early cements and/or abundance of ductile grains promoted substantial porosity destruction by compaction and the inhibition of further diagenetic modifications. The diagenetic dissolution and replacement of volcanic rock fragments and detrital feldspars by clays and albite changed the original framework composition, as well as the tectonic provenance classification of the sandstones. Detailed quantitative petrographic study allowed the reconstruction of the original detrital compositions and the distinction of six different pathways of diagenetic evolution of the sandstones, attesting to the efficiency of this method for diagenetic modelling and provenance analyses of ancient sandstones.

1. Introduction

The concept of molasse as a tectonic–sedimentary facies was first introduced by Studer (1825) for immature Miocene sandstones and conglomerates along the edge of the Swiss alpine belt. Later, Haug (1900) extended the concept to all orogenic belts. As a practical facies characterization, the usage of "molasse" or "molassic" survived the wreck of the geosynclinal theory. Molasse is now understood as a tectonofacies characterized by thick clastic deposits that accumulated in narrow basins within orogenic belts or along the borders between these belts and the craton (Van Houten, 1974). These basins are

[1] Permanent address: Universidade Federal do Rio Grande do Sul, Inst. Geociências, Dep. Mineralogia e Petrologia, Av. Bento Gonçalves, 9500, CEP 91 500, Porto Alegre, RS, Brazil.
[2] Permanent address: Unisinos, Dep. Geologia, Av. Unisinos, 950, CEP 93 020, São Leopoldo, RS, Brazil.

SSDI 0037-0738(94)00044-U

filled mostly with coarse, immature clastic sediments derived from the uplift and erosion of the orogenic belts.

Although several studies have dealt with the provenance and descriptive petrography of molassic sandstones (Füchtbauer, 1974; Maurer et al., 1982; Schwab, 1986), the precise role of detrital composition on the diagenetic evolution of molasses is poorly constrained in the literature.

The continental Cambro–Ordovician Guaritas Sequence, deposited at the end of the Brasiliano orogenic cycle in the Camaquã Basin of southern Brazil (Fig. 1), was chosen as a representative example of a continental molassic unit which enabled us to study systematically: (1) the influence of compositionally immature detrital assemblage on the diagenetic processes, (2) the diagenetic modifications of original composition and its influence on provenance interpretation, and (3) the diverse pathways of diagenetic evolution followed by the different detrital assemblages of these molasses.

2. Samples and experimental methods

93 fresh representative surface samples and 35 subsurface samples (465 m deep, cored close to basin centre) were collected from the main depositional facies of the Guaritas Sequence throughout the Camaquã Basin. 128 epoxy-impregnated thin sections were examined, and 44 of the most representative ones were selected for modal analysis by counting 300 to 400 points in each (Table 1). The detrital constituents were quantified according to the Gazzi-Dickinson method (Zuffa, 1985), where individual crystals or grains > 62 μm within the rock fragments are counted separately as mineral components, regarding their respective host rock fragments (e.g., plagioclase in intermediate volcanic rock fragments). Grain-replacive diagenetic minerals (e.g., calcite replacing K-feldspar in plutonic rock fragments) were also quantified separately to allow the reconstruction of the original detrital compositions and to characterize the interactions between framework composition and diagenesis.

The chemical composition of detrital and diagenetic minerals was analysed in twelve carbon-coated thin sections using a Cameca Camebax SX50 electron microprobe (EMP) equipped with three crystal spectrometers and a back-scattered electron detector (BSE). The operating conditions were an acceleration voltage of 8 kV for the carbonates and 12 kV for the silicates, a beam current of 6 nA and a beam diameter of 1 μm. The standards used were wollastonite (Ca and Si), MgO (Mg), $MnTiO_3$ (Mn, Ti), hematite (Fe), orthoclase (K), albite (Na) and corundum (Al). Six gold-coated samples were examined with a JEOL JSM-T330 scanning electron microscope (SEM) with an accelerating voltage of 10 kV, to elucidate the habits and the paragenetic relationships of the clay minerals and other microcrystalline diagenetic components. Five samples were reacted with anhydrous phosphoric acid at 25°C for 4 h under vacuum and the liberated CO_2 was analysed on a SIRA-12 mass spectrometer for stable O and C isotopes in the calcite cements. Analyses were converted to PDB and corrected for ^{17}O according to the procedure outlined by Craig (1957).

3. Geological setting

The Camaquã Basin, like several other Late Proterozoic/Eo–Palaeozoic basins in Africa, South America and Australia, was generated during the latest stages of development of the Brasiliano/Pan-African orogenic belts (Almeida, 1971; Porada, 1979, 1989) and corresponds to the strike-slip basins of Brito Neves and Cordani (1991). An extensional or a transtensional event at the end of the Brasiliano cycle, which led to the formation of intermontane basins, has been proposed as the tectonic setting of the Camaquã Basin during deposition of the Guaritas Sequence (Fragoso-Cesar et al., 1982, 1992; Beckel, 1990, 1992).

The Guaritas Sequence (Fig. 1) constitutes the uppermost unit of the Camaquã Basin and is bounded by major unconformities. It lies subhorizontally over older deformed molasses, and is covered by Permian cratonic sedimentary rocks of the Paraná Basin. A Cambro–Ordovician age is

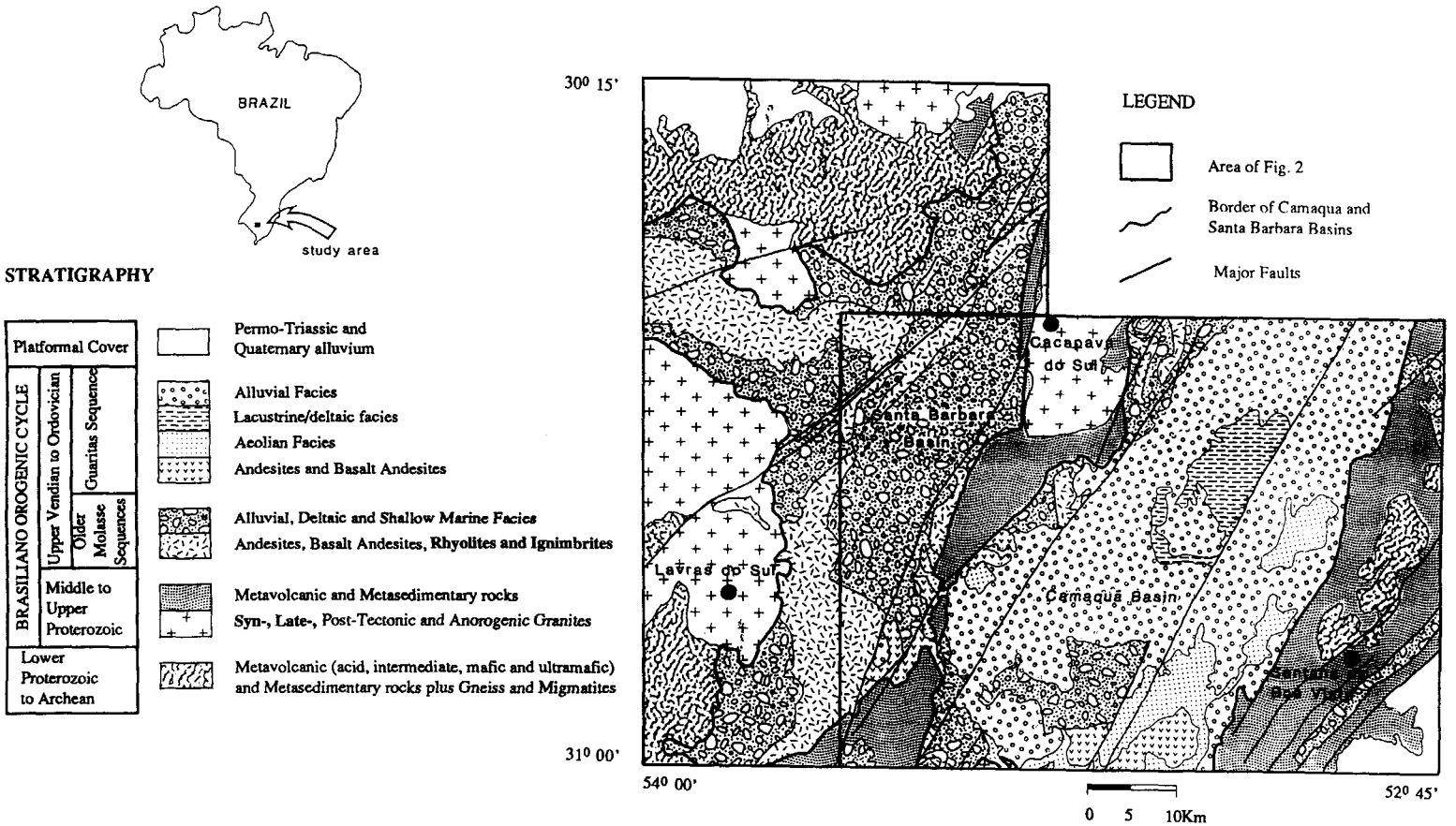

Fig. 1. Location and geological map of the Camaquã Basin in southern Brazil.

Table 1
Average modal composition of 42 Guaritas sandstones; maxima of some main constituents also recorded

Component	Average	Maximum	Component	Average	Maximum
Detrital quartz	*37.2*	*46.0*	Calcite poikilotopic	0.5	6.0
Quartz monocr.	*19.7*	*39.0*	Calcite mosaic	2.0	6.0
QzM nonundulose	8.8	–	Calcite blocky	0.1	–
Qz volcanic	1.9	–	Calcrete concretion	0.2	3.0
QzM undulose	9.0	–	Calc. in grain	0.1	–
Quartz polycr.	*10.5*	*19.1*	Calc. in det. qz	0.5	–
QzP coarse	9.2	–	Calc. in qz overgr.	0.1	–
QzP fine	0.6	–	Calc. in qz in plut.r.	0.2	–
Qz hydrothermal	0.8	–	Calc. in K-feld.	0.4	–
Qz in volc. r.f.	0.4	–	Calc. in K-fd. in pl.r.	0.1	–
Qz in plut.-gne.r.f.	4.4	–	Calc. in det plag.	0.1	–
Qz in met. r.f.	2.3	–	Calc. in plag in pl.r.	< 0.1	–
Detr. feldspar	*15.0*	*31.3*	Calc. in volc. r.f.	0.1	–
Detr. k-feld	*12.6*	*20.5*	Calc. in met. r.f.	0.1	–
K-feld. monocr.	*8.5*	*15.6*	Calc. in mica	< 0.1	–
Orthoclase	4.7	–	Calc. in heavy min.	< 0.1	–
Microcline	2.4	–	Calc. in mud intr.	< 0.1	–
Perthite	1.4	–	Calc. in pseud. matr.	0.3	–
K-feld. in volc.	0.2	–	Calc. in overszd. patch	0.1	–
K-feld. in plut.	3.8	–	Kaolinite intergr.	0.7	8.4
Detr. plagioc.	*2.4*	*4.9*	Kaol. in det. K-feld.	0.3	6.2
Plag. monocr.	*1.2*	*3.4*	Kaol. in det. Plag.	0.1	–
Plag. in plut. r.f.	1.2	–	Kaol. in Volc. r.f.	0.1	–
Fine lithics	*9.8*	*19.0*	Kaol. in mica	0.2	–
Volcanic r.f.	*5.5*	*13.0*	Kaol. in met. r.f.	0.1	–
Acid. volc. r.f.	4.7	11.8	Kaol. in pseud. matr.	0.2	–
Pyroclast. r.f.	0.3	–	Chlorite rims	0.1	–
Interm. volc. r.f.	0.5	–	Chlorite pore-fill	< 0.1	–
Metamorp. r.f.	*4.3*	*12.1*	Chl. in volc. r.f.	0.1	–
Low-grade met. r.f.	2.5	–	Illite rims	0.6	2.4
Meta-volc. r.f.	1.5	–	Illite fills	0.8	–
Meta-sedim. r.f.	0.4	–	Illite bridges	0.4	–
Sediment. r.f.	*0.1*	*1.3*	Ill. in det. K-feld.	0.1	–
Siltstone r.f.	0.1	–	Ill. in det. plag.	0.1	–
			Ill. in volc. r.f.	0.1	–
Det. accessories	*4.1*		Ill. in mud intracl.	< 0.1	–
Micas monocr.	0.9	2.1	Ill. in clay coatings	0.1	–
Micas in plut. r.f.	0.3	–	Ill. in kaolinite	0.0	–
Micas in met. r.f.	0.3	–	Ill. in pseud. matr.	0.5	4.0
Heavy minerals	0.4	4.0	Barite	< 0.1	–
Mud intraclast	0.1	–	Pyrite	< 0.1	–
Calcrete intracl.	0.4	2.8	Pyrite o/mica	< 0.1	–
Silcrete intracl.	< 0.1	–	Sulphides	< 0.1	–
Soil-alterite f.	0.2	–	Ti oxides	0.2	–
Pseudomatrix	*1.5*	*9.0*	Anatase	0.1	–
			Sphene	< 0.1	–
Diagenetic total	*28.0*	*43.5*			
Clay coatings	1.3	4.6	*Pores*		
Hematite coatings	2.4	6.0	Intergranular	3.1	9.1
Hematite pore-fill	0.8	6.0	Decompaction	0.3	–
Hem./clay pore-fill	1.9	21.0	Inter. in calcite	0.1	–
Hemat. in detr. qz	0.5	–	Inter. in hemat.	0.2	–

Table 1 (continued)

Component	Average	Maximum	Component	Average	Maximum
Hemat. in K-feld.	0.2	–	Inter. in ps. matr.	0.2	–
Hemat. in plag.	< 0.1	–	Intragr. in k-fd.	1.0	–
Hemat. in volc. r.f.	0.8	–	Intragr. in plag.	0.3	–
Hemat. in biotite	0.3	–	Intragr. in volc. r.f.	0.6	–
Qz overgrowth	3.5	19.5	Moldic	< 0.1	–
Qz discrete crystal	0.5	4.4	Fracture	< 0.1	–
Qz in volc. r.f.	0.1	–	Shrinkage	0.1	–
K-feld. overgr.	< 0.1	–	Oversized	< 0.1	–
K-feld. discr. cryst.	0.1	–	*Macropores total*	*5.9*	*15.7*
K-fd. in detr. K-fd.	0.1	–	Micropores	common	abundant
Albite overgr.	< 0.1	–			
Albite discrete cr.	0.1	–	Intergr. vol.	19.4	29.6
Alb. in K-feld.	2.2	–	Grain vol.	80.6	92.9
Alb. in plag	3.0	–	Replac. total	12.1	21.9
Alb. in K-fd.in pl.r	0.4	–	*Packing*	*56.0*	*95.0*
Alb. in plag.in pl.r.f.	0.7	–		P minimum	32.0

estimated from radiometric dates of intercalated andesitic flows and illitic clays in mudrocks (Bonhome and Ribeiro, 1983; Soliani et al., 1984; Fragoso-Cesar et al., 1984).

The sequence is about 300 m thick, comprising mostly coarse clastic rocks with volcanic intercalations near the base. The volcanic rocks (basaltic andesites) represent the last magmatic event in the basin and are related to a high-K, calc-alkaline to shoshonitic volcanism. The older molassic units include andesites, andesitic basalts, rhyolites and ignimbrites related to high-K, metaluminous, calc-alkaline magmatism (Almeida et al., 1992).

4. Depositional systems

Several authors have proposed a continental semi-arid environment for the Guaritas Sequence, characterized by the association of alluvial-fan and braided alluvial plain deposits with aeolian and lacustrine–deltaic sediments and volcanic intercalations near its base (Becker and Fernandes, 1982; Fragoso-Cesar et al., 1984; Jost, 1984; Lavina et al., 1985; Beckel, 1990; Paim, 1992). The basin-wide facies mapping of the sequence (Paim, 1993) confirmed these previous interpretations and illustrated the alluvial–aeolian–deltaic facies association (Figs. 1 and 2).

The basin-wide analysis of the depositional structures and textures of the alluvial facies (Paim, 1993) suggest an objective delineation of two distinct domains (Fig. 2): (1) a tributary alluvial-fan system (*sensu* Rust and Koster, 1984) fed from the eastern border of the basin and characterized by two main fan lobes which show a clear association with structural lows of the adjacent basement; and (2) a braided trunk river system (*sensu* Rust and Koster, 1984) located in the western side of the basin with palaeocurrents to the southwest. The lateral variation of the mean grain size suggests an intermittent reworking by these rivers of alluvial-fan deposits, originally fed transversally from the western border of the basin (Fig. 2).

Aeolian deposits are more common in the lower levels of the sequence (Fig. 1). Lacustrine facies are spread mostly in the middle part of the sequence, being associated with the development of fan-deltas fed from the western border, and braid-delta plain related to the braid trunk river system (Figs. 1 and 2).

5. Textural evidence of recycling

The textural characteristics of the Guaritas Sequence reflect the dynamics of the depositional systems and the tectonic setting. The marginal

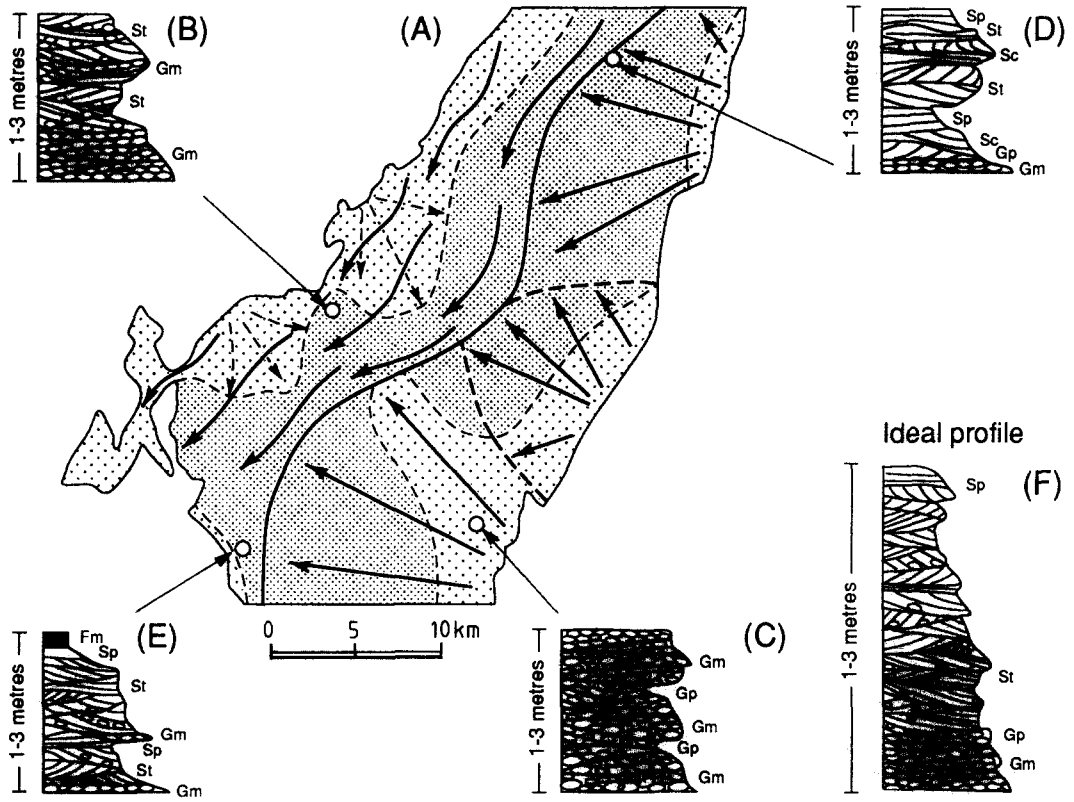

LEGEND

Alluvial Palaeogeography

- Sandy alluvial deposits
- Mixed alluvial deposits
- Boundary between trunk rivers and tributary fans
- Braided river streams
- Tributary fan streams
- Reworked tributary fans
- Tributary fan lobe boundaries

Sedimentary Structures

- Trough Cross Stratification
- Horizontal Lamination
- Convolute Bedding

Lithologies

- Conglomerates
- Sandstones
- Pelites

Facies Codes Gm, St modified after Miall (1978)

Fig. 2. Patterns of depositional palaeocurrents and typical facies associations of Guaritas alluvial deposits in the Camaquã Basin.

conglomerates (proximal alluvial-fan deposits) and the fluvial conglomerates and conglomeratic sandstones along the centre of the basin (distal tributary alluvial-fan and part of the trunk braid river system) show a characteristic mixture of populations with very heterogeneous roundness. This is related to a mixing of particles recycled from the older molassic units with first-cycle sediments derived from the adjacent crystalline basement. The poorly sorted fluvial sands, deposited by high-energy currents crossing a relatively narrow basin, show conspicuous rounding heterogeneity related to the recycling of grains from the older molassic units and from the aeolian deposits, the latter being probably the source of the very well-rounded grains. In the aeolian sandstones, the development of the typical foreset texture is incipient, meaning a relatively poorly defined granulometric lamination, and heterogeneous rounding, which indicates a rapid and incomplete aeolian reworking of the fluvial sands.

6. Detrital composition

Like many other molasses (Schwab, 1986), the Guaritas sediments are mostly lithic arkoses and litharenites (Fig. 3) containing fragments of a large variety of rocks derived from the orogenic belt, from the adjacent craton, from older uplifted molassic units, and from extrabasinal and intrabasinal volcanics. Detrital quartz types include: metamorphic polycrystalline and strongly undulose monocrystalline grains; plutonic slightly undulose monocrystalline grains; volcanic monocrystalline grains with abrupt extinction, euhedral shape and/or embayments; and hydrothermal milky quartz with abundant fluid inclusions. The relatively low amounts of quartz in the Guaritas sandstones (original average (o.a.) 31%, exceptionally up to 46% in some aeolian deposits; Table 1) indicate the compositional immaturity typical of molassic deposits.

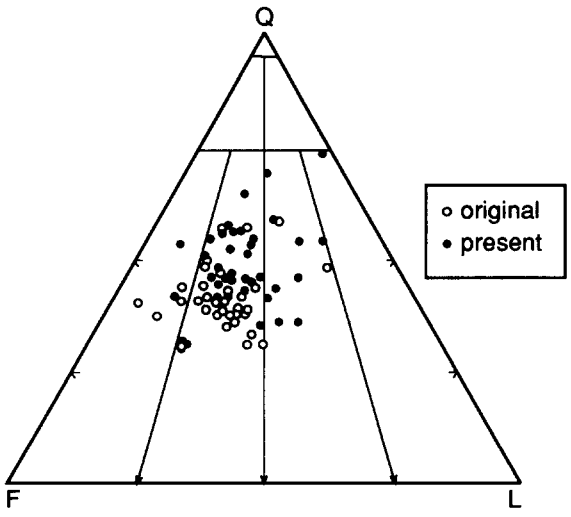

Fig. 3. Present and original detrital composition of 42 Guaritas sandstone samples plotted on Folk's (1968) diagram.

The sandstones are relatively rich in feldspars (7 to 31%; o.a. 20%). K-feldspars (o.a. 13%) dominate over plagioclases (o.a. 5%). Most of the orthoclase, sanidine and plagioclase grains are strongly altered to sericite/illite, albite or kaolinite, whereas others are fresh. The strong differential alteration of feldspars is related to alteration that occurred in the source areas under retrograde metamorphism, hydrothermal activity, or diagenesis of the crystalline basement and of the older molasses. These mixtures of detrital feldspars and the heterogeneous replacement of detrital by authigenic feldspars precluded the utilization of systematic optical and X-ray techniques for provenance analyses (Suttner and Basu, 1977; Plymate and Suttner, 1983).

The sandstones are rich in rock fragments (o.a. 15% of fine-grained rock fragments, 25% of total lithoclasts; Table 1). Plutonic (granitic and gneissic) lithoclasts averaged originally 11%. Volcanic lithoclasts (trace to 13%, o.a. 8%) are dominantly rhyolites with felsitic textures, including intermediate/basic types commonly with trachytic or porphyritic textures, acidic vitric tuffs and ignimbrites. The distribution of volcanic rock fragments relative to total framework grains (Fig. 4) shows a pattern indicating a main input from the western margin of the basin. This pattern was inherited from the original transversal alluvial-fans that were subsequently reworked by the longitudinal trunk streams (Fig. 2). These fragments were derived from the volcanic intercalations in the older molassic sequences, particularly the ex-

tensive acidic and intermediate volcanic areas to east and west of Lavras do Sul city, and from the andesites intercalated at the base of the Guaritas Sequence (Fig. 1). The concentrations of rhyolitic grains in the basal aeolian deposits along the eastern margin are connected most probably with the higher resistance to abrasion of these fragments in relation to other lithoclasts and feldspars.

Metamorphic lithoclasts (slate, phyllite, schist, meta-volcanite, meta-sandstone, meta-siltstone and marble) are disseminated throughout the

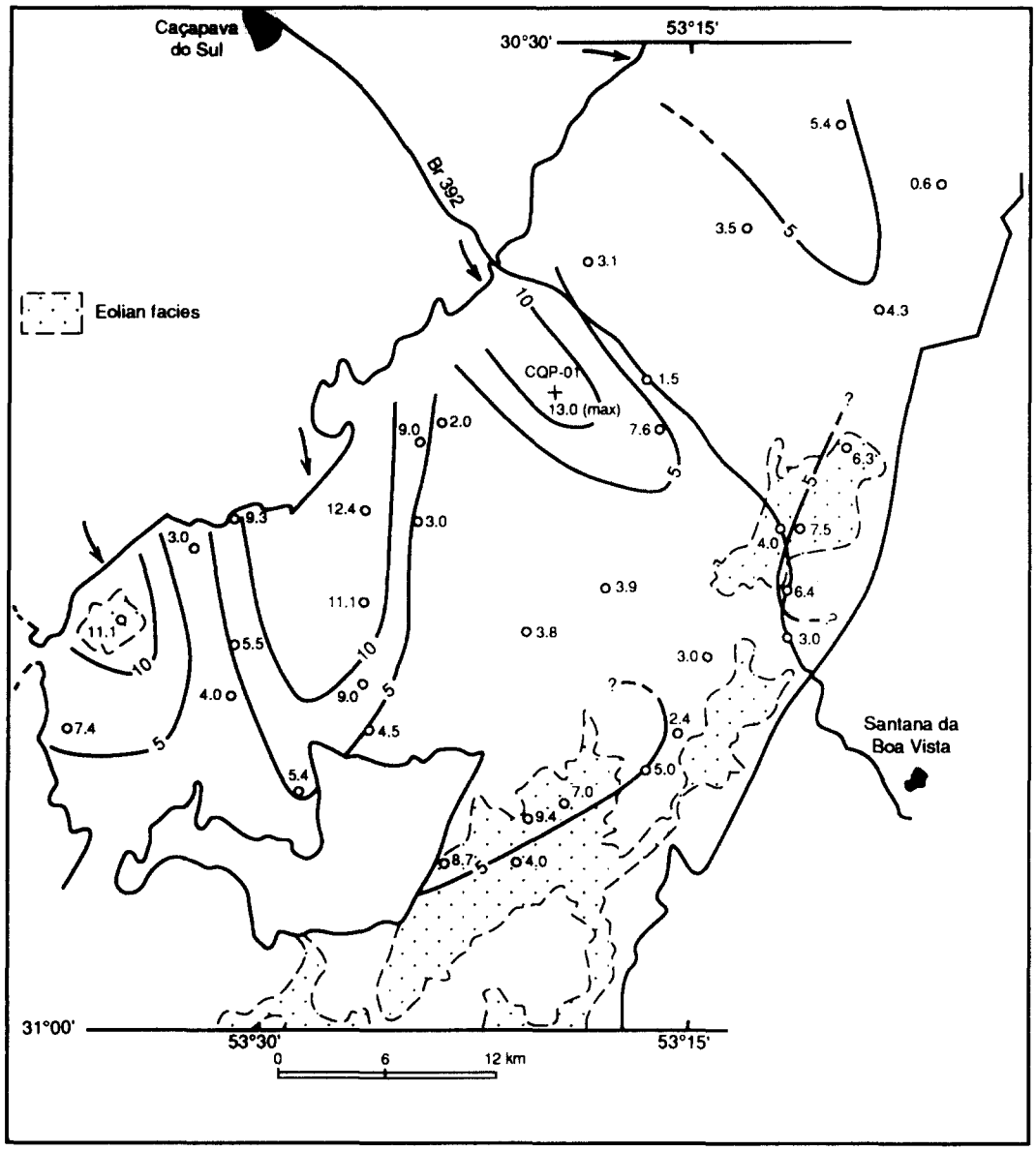

Fig. 4. Map of the distribution of volcanic rock fragments in the Guaritas sandstones (normalized for total framework = 100%). Observe the pattern inherited from the original alluvial systems from the western margin (nevertheless preserved from the reworking by longitudinal braid trunk fluvial system), and localized aeolian concentrations of rhyolite fragments to the east.

basin. The original average of 7% (trace to 12.1%; Table 1) is underestimated, because part of the pseudomatrix was formed through compaction of micaceous metamorphic rock fragments. The source areas are the fold-thrust belt of the Santana da Boa Vista area (eastern margin) and the Caçapava do Sul High (western margin of the basin; Fig. 1). The distribution pattern of total metamorphic lithoclasts in the sandstones (Fig. 5) reflects the alluvial-fans coming from the Caçapava High, and subordinately, in the northeastern area, from the fold belt to the north of Santana. The input from the southeast border is masked by the larger erosion and dominant out-

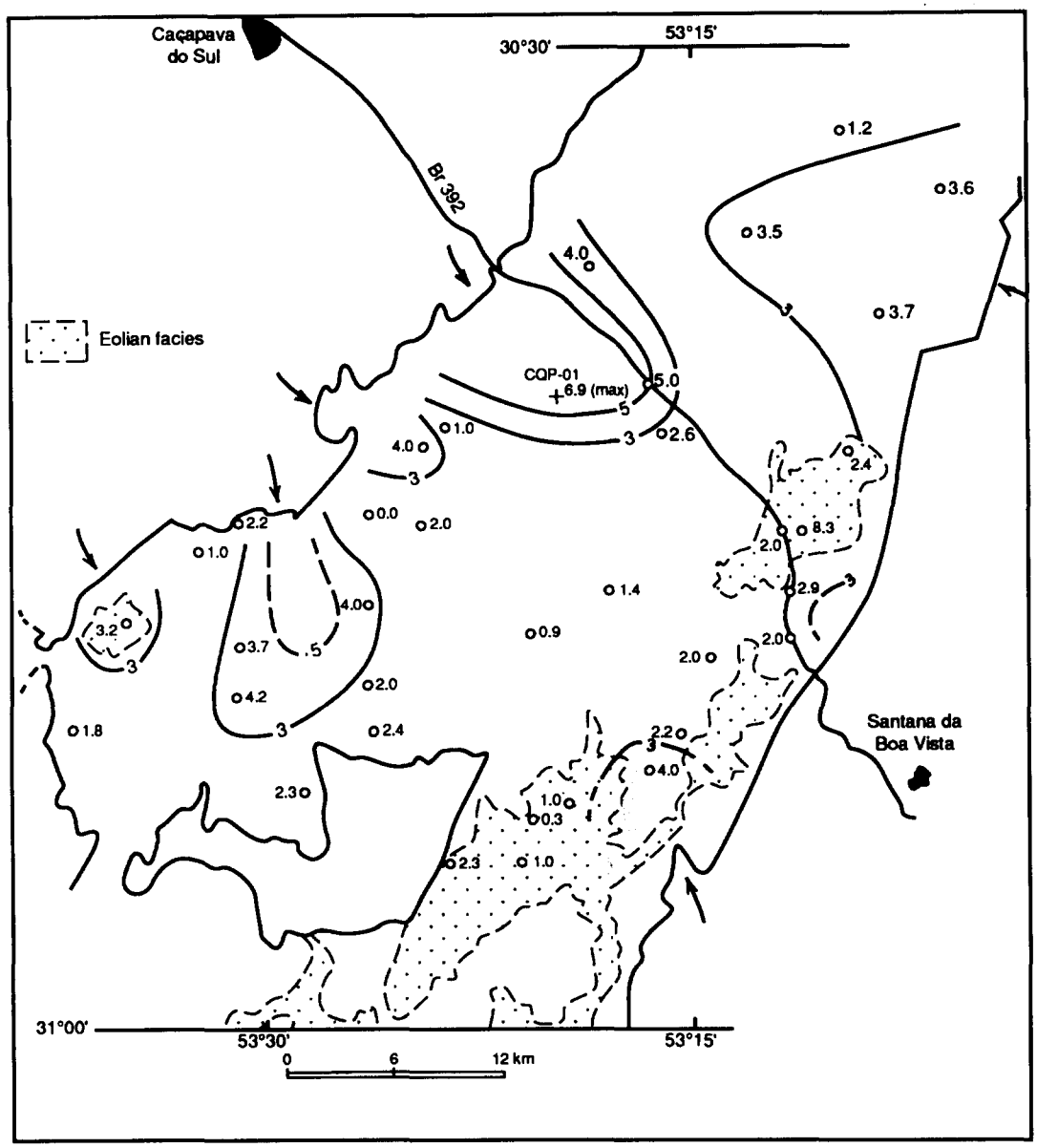

Fig. 5. Map of the distribution of metamorphic rock fragments in the Guaritas sandstones (normalized for total framework = 100%). Pattern of main alluvial input from the Caçapava High, to the west, and Santana High, to the east.

cropping of basal aeolian sandstones in the area, but is obvious in the conglomerates. Commonly, proximal fanglomerates along the basin margins show oligomict compositions (phyllite or quartz–schist conglomerates) derived from immediately adjacent source areas. Sedimentary lithoclasts, mostly siltstones and sandstones eroded from older molassic units (Fig. 1), are scarce and randomly disseminated.

Despite the evident original immaturity of the deposits, relatively few types of accessory detrital minerals have survived. The latter are mostly garnet, epidote, ilmenite, magnetite and the more stable zircon, rutile, tourmaline, and apatite (present total average 0.4%, maximum 4%). Pyroxene, amphibole, staurolite, sillimanite, and other heavy minerals of metamorphic affiliation that are abundant in the source rocks are rare in the sandstones. The most abundant accessory minerals are micas, which are concentrated mostly in the fine sandstones and siltstones (maximum more than 10%; o.a. 1% and maximum 2% in the coarser quantified sandstones). Muscovite predominates over biotite, the latter of which is commonly altered to hematite.

Mud intraclasts are common in the Guaritas sandstones. Intraformational conglomerates of fragments eroded from abandoned channel-fill or lacustrine deposits occur at the base of many alluvial cycles. Fragments of shallow-phreatic calcite with included hematite and sand/silt grains (calcretes), or of microcrystalline quartz and chalcedony (silcretes) are common. The abundance of intraclasts in several levels of the Guaritas is related to the rapid lateral channel migration. Present amounts of intraclasts, average of 0.5%, is clearly underestimated, considering that pseudomatrix was produced mostly by the compaction of mud intraclasts, and that the major concentrations are segregated in the intraformational conglomerates at the base of the depositional cycles.

7. Early diagenetic environment

Palaeoclimate exerts a very important control on the detrital composition and on the near-surface diagenetic environment of continental sandstones (Dutta and Suttner, 1986; Suttner and Dutta, 1986). The palaeolatitude of the Camaquã Basin during the Late Cambrian to Middle Ordovician was around 30°S (Scotese and Barret, 1990), which placed it within the subtropical dry belt characterized today by the largest concentration of deserts (Paim and De Ros, in prep.). The survival of chemically unstable grains, such as the vitric volcanic fragments, indicates that the regional climate was dominantly dry during deposition of the Guaritas Sequence (cf. Suttner and Dutta, 1986). Other lines of evidence for the aridity of the climatic conditions include the widespread aeolian reworking and the occurrence of infiltrated clays and shallow-phreatic calcite and silcrete. The depositional characteristics of the alluvial deposits support the interpretation of a regional semi-arid climate with prolonged dry intervals and episodic floods (Paim, in prep.; Paim and De Ros, in prep.). Many of the diagenetic processes in Guaritas sandstones reveal the role of this semi-arid continental climate in the interactions between meteoric waters and the immature detrital mineralogy.

8. Burial history

Estimation of the maximum burial of the sequence is difficult because post-Cambro–Ordovician sequences have been totally eroded from the centre of the Camaquã Basin. The eroded edge of the Permian Tubarão Group of the intracratonic Paraná Basin, however, covers the northern margin of the Camaquã Basin, and several remnants of Permian shales, coals and sandstones are scattered over the basement in adjacent areas. These features indicate that the centre of the Camaquã Basin was also covered by some hundreds of metres of Late Palaeozoic–Early Mesozoic cratonic sediments. The vitrinite reflectance of coals from the Permian Tubarão Group that overlay nearby areas of the basement indicates a maximum thickness of less than 1000 m for the Permian cover of the Camaquã Basin. Assuming present geothermal gradients in Paraná Basin

(25–30°C/km; Zembruscki and Chang, 1989), this maximum overburden would correspond to maximum temperatures of 50 to 60°C.

Burial diagenetic processes had a relatively limited intensity in the Guaritas sandstones despite their age, tectonic setting and immature mineral composition. This is attributed to the limited maximum burial and to the permeability and porosity reduction by the near-surface processes of precipitation and infiltration. The erosion of the Permian cover of the Guaritas Sequence induced limited telodiagenetic (*sensu* Schmidt and McDonald, 1979) processes of decompaction, evidenced by the presence of lamellar pores along grain–cement and grain–grain contacts. Telodiagenesis has also promoted locally the precipitation of hematite on burial calcite and illite. Some dissolution and kaolinization of feldspars and volcanic rock fragments, when not associated to burial illite, quartz and albite, are also possibly telogenetic.

9. Diagenetic mineralogy

The main diagenetic constituents in Guaritas sandstones and conglomerates include, approximately in paragenetic sequence, the following.

9.1. Hematite

Hematite displays four occurrence habits:

(1) Cryptocrystalline coatings on detrital grains, commonly intergrown with mixed-layer illite/smectite (I/S).

(2) Pore-filling intergranular aggregates, mostly around biotite and heavy-mineral grains, which were the main source of iron for the hematite (cf. Walker, 1967; Turner and Archer, 1977; Morad, 1983). The sandstones contain on average 2% hematite coatings and 1% pore-fillings (up to 10%; Table 1).

(3) Curled fragments of hematite coatings alternating with rims of I/S (Fig. 6a). These aggregates (average 2%) are particularly abundant (up to 21%) in levels with abundant dissolved garnet, epidote, hornblende and other heavy minerals, and vitric volcanic fragments (Fig. 6a). The probable stages involved in the generation of the hematite–clay aggregates (Fig. 7) are: (a) unstable grains were altered at near-surface to a mixture of cryptocrystalline iron oxyhydroxides (e.g. goethite) (b) and smectite (c), as described by Walker et al. (1978) for Cenozoic alluvium of semi-arid North America; (d) during burial, the oxyhydroxide coatings where dehydrated to hematite (cf. Walker, 1967), resulting in shrinkage, fragmentation, curling, and the clays were recrystallized (e) to well-developed "honeycomb" rims of I/S arranged perpendicular to the surfaces of the coatings (Fig. 7; Fig. 6a).

(4) As replacement of volcanic rock fragments, biotite flakes, heavy minerals and feldspar grains.

Hematite is causing the general red colour of Guaritas sandstones, and is typical of near-surface diagenesis in continental semi-arid fluvial environments with repeated fluctuation of the water table (cf. Walker, 1967).

9.2. Infiltrated clays

Clay coatings average 1% of bulk volume of sandstones and conglomerates (0–5%; Table 1), being made of platelets oriented tangentially to the grain surfaces (Fig. 6b), and usually intergrown with hematite. The coatings are irregular, anisopachous and show the characteristic features of mechanically infiltrated clays (Fig. 6b; Moraes and De Ros, 1990). These clays are introduced during near-surface diagenesis of continental sediments under semiarid conditions by episodic floods. Large volumes of detrital clays can be introduced in originally clean alluvium by this process (Walker, 1976; Walker et al., 1978; Matlack et al., 1989; Moraes and De Ros, 1990). The limited amounts and irregular distribution of the infiltrated clays in the Guaritas sandstones indicate a rapid and continuous migration of the fluvial channels during deposition, which has prevented repeated infiltration in the same areas.

Detrital clays from Recent semi-arid environments are dominantly smectitic (Keller, 1970; Walker et al., 1978) and are commonly transformed during burial and diagenesis to I/S or chlorite/smectite clays (Moraes and De Ros, 1990). SEM investigation indicates that infiltrated

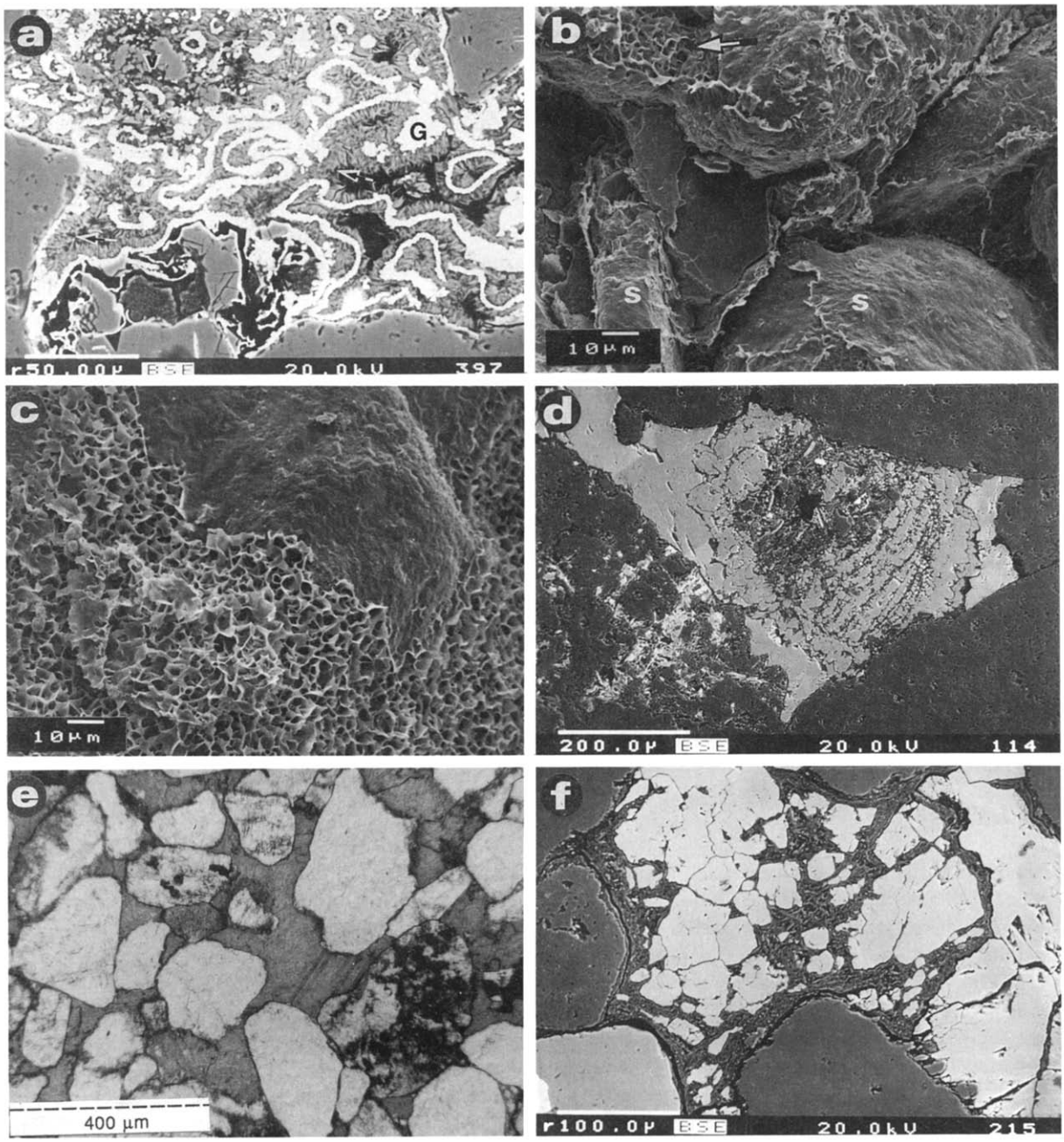

Fig. 6. (a) BSE image of detached and curled hematite coatings (bright) engulfed by rims of I/S clay aggregates (arrows) around dissolved remnants of garnet (*G*) and volcanic (*V*) grains. (b) SEM image of infiltrated clay coatings, showing original smooth, cryptocrystalline smectite texture (*S*) partially replaced and covered by authigenic I/S (arrow). (c) SEM photo of infiltrated clay coatings being replaced and covered by honeycomb-shape authigenic I/S clays; original smectite texture preserved along intergranular contact area. (d) BSE image of shallow phreatic calcite showing homogeneous Mn- and Fe-free composition precipitated around a laminated calcrete intraclast core, and followed by slightly brighter Mn-enriched intergranular burial calcite; concentric zonation is due to micropores and hematite. (e) Uncrossed-polarizers micrograph showing heterogeneity of packing in area cemented by coarse calcite (stained). (f) BSE image of blocky calcite replacing illitized pseudomatrix.

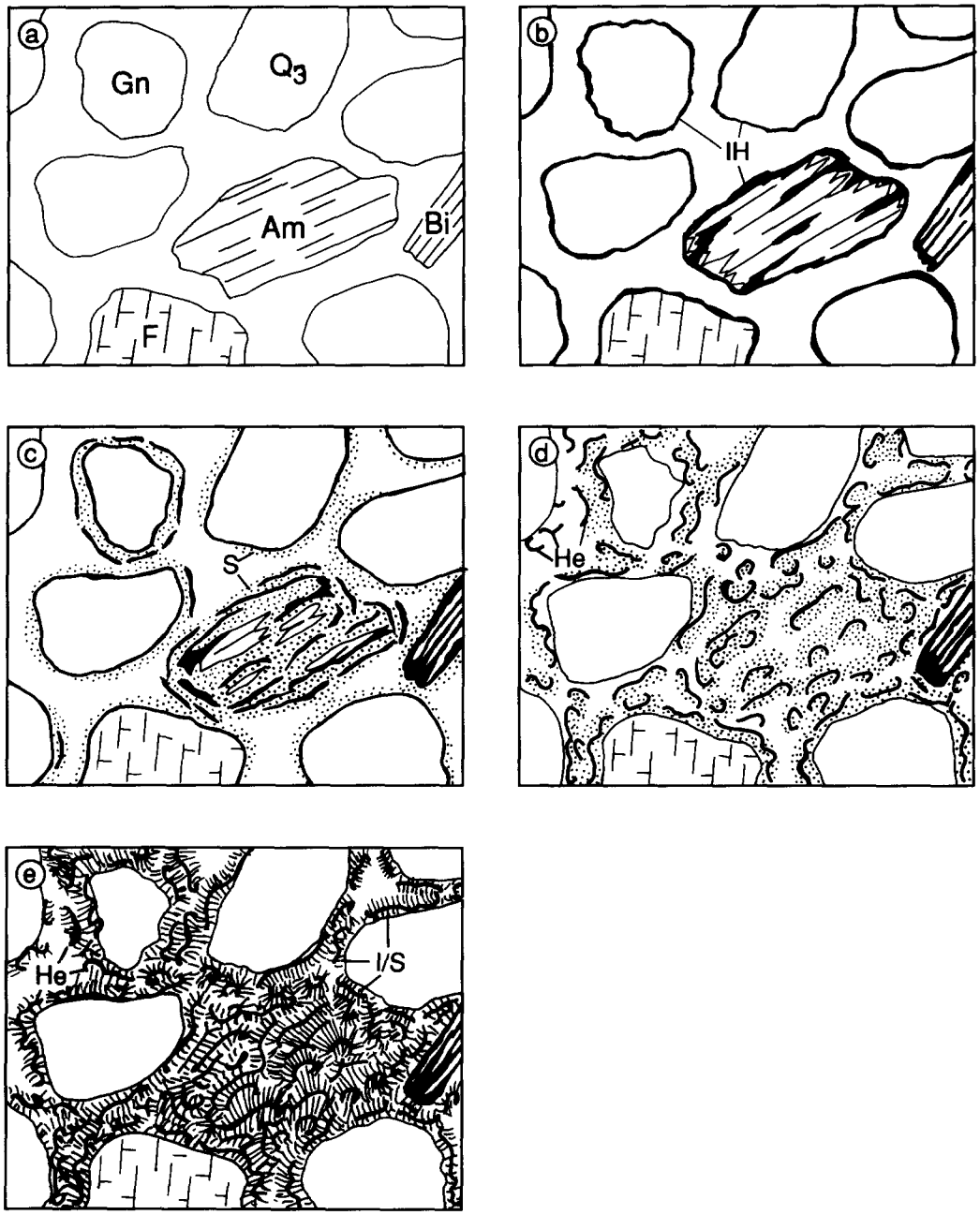

Fig. 7. Schematic sketch of the steps involved in the generation of hematite–clay aggregates through the near-surface alteration of heavy minerals: (a) immature sand with quartz (*Qz*), feldspar (*F*), garnet (*Gn*), amphibole (*Am*) and biotite (*Bi*) grains; (b) incipient alteration of biotite and amphibole and precipitation of iron hydroxide (*IH*) coatings over the grains; (c) proceeding alteration and dissolution of heavy-mineral grains, with precipitation of finely crystalline smectite (*S*); (d) shrinkage, fragmentation and curling by the dehydration of hydroxides to hematite (*He*) and of smectite; (e) illitization of smectite and neoformation of fringing I/S.

smectites in the Guaritas Sequence were extensively replaced and/or covered by authigenic I/S and illite. This transformation is visible by the gradual upturning and curling of edges of the smooth smectite coatings, followed by the neoformation of I/S alveolar aggregates (Fig. 6c) and finally, the precipitation of fibrous illite (Keller et al., 1986). The original smooth texture of the detrital finely crystalline smectites can still be recognized mostly along the areas of intergranular contacts (Fig. 6c).

9.3. Calcite

Calcite occurs in two main habits:

(1) Small, scattered (< 2 mm of diameter; 0–3%; average 0.2%) concretionary aggregates with microcrystalline, radial–concentric optical zonation and displacive texture (Fig. 6d). Strong and Milodowski (1987) interpreted similar aggregates in Triassic fluvial sandstones of the Wessex Basin, U.K. as precipitated intermittently under minimal overburden. Microprobe analyses revealed that this calcite has a homogeneous composition with very low (< 0.05%) Fe, Mn and Mg contents, and that the optical zonation is due to inclusions of hematite and micropores (Fig. 6d). The concentric displacive arrangement of the microcrystalline calcite indicates precipitation in the shallow phreatic zone. Vadose precipitation would produce geopetal pendular or meniscus geometries. The microcrystalline calcite commonly nucleated over intraclasts of microcrystalline calcite, which are commonly laminated and including silt grains and hematite (Fig. 6d). These fragments were eroded by the alluvial currents from near-surface calcite crusts (calcrete) formed in fine channel-fill and lacustrine sediments. The development of calcrete in alluvial sediments under semi-arid climatic conditions is well reported in the literature (Leeder, 1975; Wright and Tucker, 1991).

The $\delta^{18}O_{PDB}$ values range between −9.5 and −8.5‰, which is typical of meteoric waters (Table 2). The $\delta^{13}C_{PDB}$ values between −1.5 and −1.0‰ reflect exclusively the atmospheric CO_2 composition due to the absence of land vegetation during the Cambro–Ordovician. Today's atmospheric CO_2 has a $\delta^{13}C_{PDB}$ value of −7‰ and is in equilibrium with carbonate compositions of about −2‰ (PDB) (Platt, 1992). The observed slight enrichment in ^{13}C is probably reflecting a fractionation related to evaporation under the semi-arid continental palaeoenvironment (cf. Suchecki et al., 1988).

(2) Coarsely crystalline mosaic to poikilotopic calcite, which averages 2.5% of the bulk-rock volume (0–6%), has commonly nucleated on microcrystalline calcite concretions and intraclasts. EMP revealed an enrichment in Mn (up to 0.88%). The crystals show homogeneous composition or subtle zonation by gradual and slight increase in Mn from the cores outwards. Areas cemented by coarse calcite show locally heterogeneous packing (Fig. 6e), suggesting that the precipitation initiated during compaction. Burial calcite has marginally replaced on average 1.6% of the detrital grains (Table 1) and clay pseudomatrix as blocky crystals (Fig. 6f). The $\delta^{13}C_{PDB}$ values (−2.5 to −1‰; Table 2) are similar to those of the near-surface calcite. If the isotopic values can be considered representative of the two calcite textures, such similarity indicates derivation by dissolution–reprecipitation of the near-surface cements. The similar $\delta^{18}O_{PDB}$ values (−10 to −8‰; Table 2) indicate that this recycling occurred still at relatively low temperatures, under relatively shallow burial.

9.4. Barite

Barite occurs as small aggregates of lath-shaped crystals (average < 0.1%) which show

Table 2
Stable oxygen and carbon isotopic composition of Guaritas Sequence calcites

	SPh	SPh	CB	CB	CBCI
$\delta^{18}O$ SMOW	21.40	22.15	22.64	20.69	21.17
$\delta^{18}O$ PDB	−9.22	−8.50	−8.02	−9.92	−9.45
$\delta^{13}C$ PDB	−1.47	−0.99	−0.99	−2.21	−1.78

SPh: shallow-phreatic microconcretions; CB: coarse burial calcite; CBCI: 2% coarse burial calcite and 3% shallow phreatic (calcrete) intraclasts.

slight dissolution and replacement by engulfing burial calcite. Barite thus precipitated during late near-surface or early burial diagenesis. Ba ions needed for barite precipitation were apparently derived from the dissolution and replacement of detrital K-feldspar by clays.

9.5. Quartz

Thick quartz overgrowths (up to 250 μm) average 3.5% in the Guaritas sandstones (Table 1). Some fluvial sandstones along the basin centre contain up to 13% quartz overgrowths (Fig. 8).

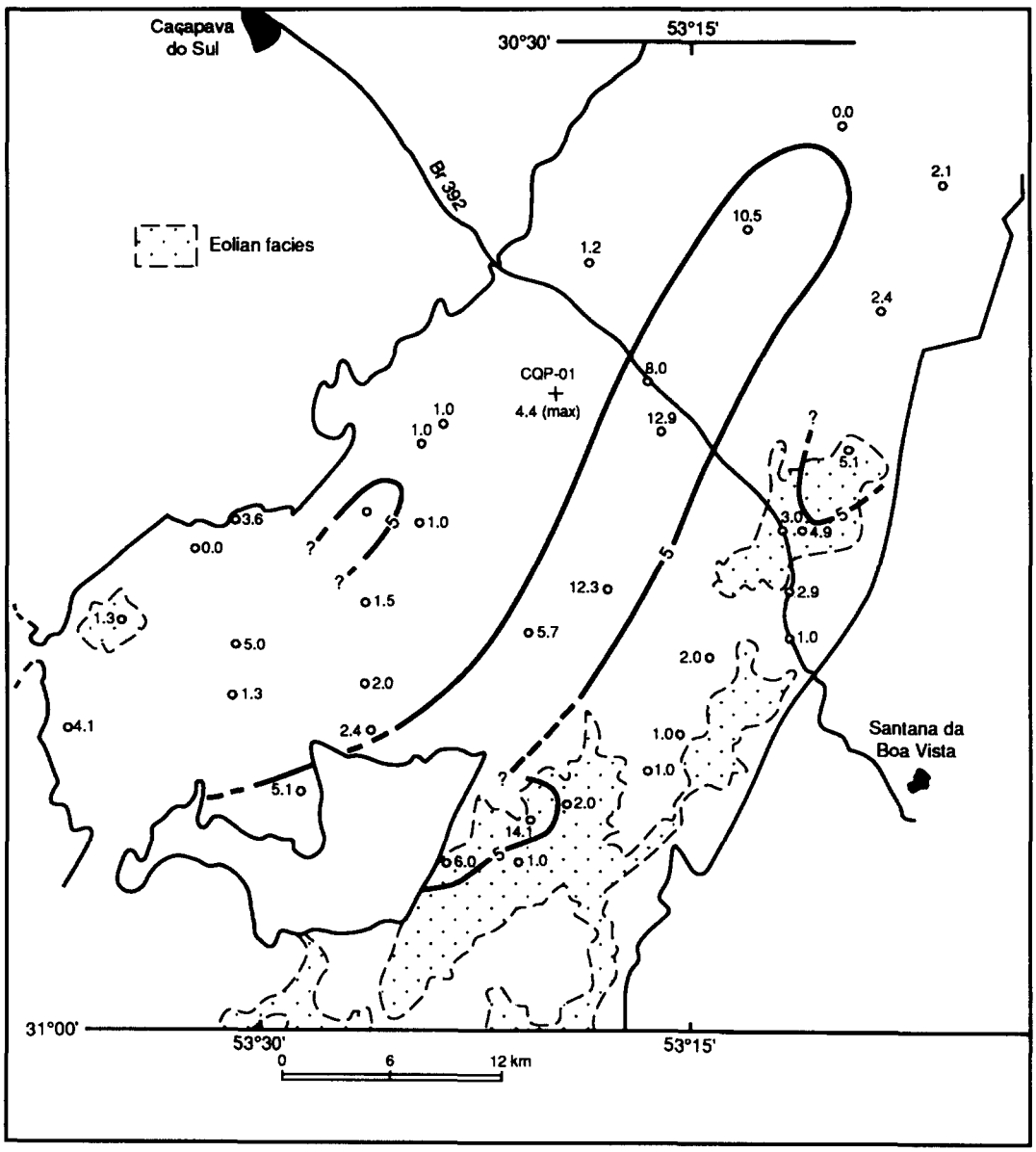

Fig. 8. Map of the distribution of quartz cement in the Guaritas sandstones. Larger amounts in the more reworked fluvial sandstones along the centre of the basin, and in aeolian sandstones.

Table 3
Average modal composition of 16 aeolian and reworked fluvial, and 26 alluvial sandstones of Guaritas Sequence (compare amounts of detrital quartz, volcanic rock fragments, quartz and calcite cements, and packing)

Component	Aeolian + rew. fluv.	Alluvial	Component	Aeolian + rew. fluv.	Alluvial
Detrital quartz	38.6	36.4	Calcite poikilotopic	0.1	0.8
Quartz monocr.	21.1	18.9	Calcite mosaic	1.5	2.2
QzM nonundulose	9.5	8.4	Calcite blocky	< 0.1	0.3
Qz volcanic	2.3	1.7	Calcrete concretion	< 0.1	0.1
QzM undulose	9.4	8.7	Calc. in grain	0.2	0.8
Quartz polycr.	11.3	10.1	Calc. in det qz	0.1	0.1
QzP coarse	9.7	8.8	Calc. in qz overgr.	< 0.1	0.2
QzP fine	0.4	0.6	Calc. in qz in plut.r.	0.2	0.5
Qz hydrothermal	1.1	0.6	Calc. in K-feld.	< 0.1	0.1
Qz in volc. r.f.	0.4	0.3	Calc. in K-fd. in pl.r.	< 0.1	0.1
Qz in plut.-gne.r.f.	3.7	4.8	Calc. in det. plag.	< 0.1	0.0
Qz in met. r.f.	2.2	2.4	Calc. in plag in pl.r.	< 0.1	0.1
Detr. feldspar	14.0	15.6	Calc. in volc.r.f.	< 0.1	0.2
Detr. K-feld.	12.2	12.9	Calc. in met. r.f.	< 0.1	< 0.1
K-feld. monocr.	8.5	8.5	Calc. in mica	< 0.1	< 0.1
Orthoclase	4.4	4.9	Calc. in heavy min.	< 0.1	< 0.1
Microcline	2.5	2.4	Calc. in mud intr.	< 0.1	0.4
Perthite	1.5	1.3	Calc. in pseud. matr.	< 0.1	0.1
K-feld. in volc.	0.3	0.2	Calc. overszd. patch	1.2	0.5
K-feld. in plut.	3.3	4.1	Kaolinite intergr.	0.6	0.1
Detr. plagioc.	1.8	2.8	Kaol. in det. K-feld.	0.2	< 0.1
Plag. moncr.	0.9	1.5	Kaol. in det. plag.	0.1	0.1
Plag. in plut. r.f.	0.9	1.3	Kaol. in volc.r.f.	0.3	0.1
Fine lithics	10.1	9.7	Kaol. in mica	0.2	0.1
Volcanic r.f.	6.4	4.9	Kaol. in pseud. matr.	0.2	0.3
Acid. volc. r.f.	5.4	4.2	Chlorite rims	0.2	< 0.1
Pyroclast. r.f.	0.5	0.3	Chlorite pore-fill	< 0.1	< 0.1
Interm. volc. r.f.	0.5	0.5	Chl. in volc.r.f.	< 0.1	< 0.1
Metamorp. r.f.	3.7	4.6	Illite rims	0.6	0.6
Low-grade met. r.f.	2.0	2.7	Illite fills	< 0.1	0.1
Meta-volc. r.f.	1.2	1.6	Illite bridges	0.4	0.4
Meta-sedim. r.f.	0.5	0.3	Ill. in det. K-feld.	0.2	< 0.1
Sediment. r.f.	< 0.1	0.1	Ill. in det. plag.	0.2	< 0.1
Siltstone r.f.	< 0.1	0.1	Ill. in volc. r.f.	0.1	< 0.1
			Ill. in mud intracl.	< 0.1	< 0.1
Det. accessories	3.2	4.7	Ill. in clay coatings	0.2	< 0.1
Micas Monocr.	0.7	1.1	Ill. in kaolinite	< 0.1	< 0.1
Micas in plut. r.f.	0.2	0.4	Ill. in pseud. matr.	0.3	0.7
Micas in met. r.f.	0.2	0.3	Barite	< 0.1	< 0.1
Micas in sed. r.f.	0.2	0.5	Pyrite	< 0.1	< 0.1
Heavy minerals	0.1	0.1	Pyrite o/mica	< 0.1	< 0.1
Mud intraclast	0.2	0.5	Sulphides	< 0.1	< 0.1
Calcrete intracl.	< 0.1	0.0	Ti oxides	0.2	0.3
Silcrete intracl.	0.2	0.2	Anatase	< 0.1	< 0.1
Pseudomatrix	1.5	1.5	Sphene	< 0.1	< 0.1
Diagenetic total	28.3	27.8	*Pores*		
Clay coatings	1.6	1.1	Intergranular	3.1	3.1
Hematite coatings	2.2	2.5	Decompaction	0.2	0.3
Hematite pore-fill	0.8	0.8	Inter. in calcite	< 0.1	0.2
Hem./clay pore-fill	0.0	3.1	Inter. in hemat.	< 0.1	0.3

Table 3 (continued)

Component	Aeolian + rew. fluv.	Alluvial	Component	Aeolian + rew. fluv.	Alluvial
Hemat. in detr. qz	0.4	0.5	Inter. in ps. matr.	0.1	0.2
Hemat. in K-feld.	0.2	0.2	Intragr. in K-feld	1.1	1.0
Hemat. in plag.	< 0.1	< 0.1	Intragr. in plag.	0.5	0.2
Hemat. in volc. r.f.	0.8	0.8	Intragr. in volc. r.f.	0.7	0.5
Hemat. in biotite	0.3	0.3	Moldic	< 0.1	< 0.1
Qz overgrowth	6.8	1.5	Fracture	< 0.1	< 0.1
Qz discrete crystal	0.8	0.3	Shrinkage	< 0.1	0.1
Qz in volc.r.f.	0.2	0.0	Oversized	< 0.1	< 0.1
K-feld. overgr.	< 0.1	< 0.1	*Macropores total*	5.9	5.9
K-feld. discr. cryst.	< 0.1	0.1			
K-fd. in detr.K-feld.	0.1	0.0	Micropores	rare	common
Albite overgr.	< 0.1	< 0.1			
Albite discrete cr.	0.2	0.1	Intergr. vol.	20.3	18.8
Alb. in K-feld.	2.1	2.2	Grain vol.	79.7	81.2
Alb. in plag.	2.9	3.0	Replac. total	11.9	12.3
Alb. in K-fd. in pl.r.	0.2	0.5	*Packing*	46.4	57.5
Alb. in plag. in pl.r.f.	0.6	0.7	Grain size	medium	coarse

This distribution was probably related to three factors. First, silica concentration of the groundwaters, supplied by the dissolution of volcanic and other unstable grains, increased towards the basin centre and was enhanced by evaporation. Second, the higher amount of detrital quartz in the more reworked sands provided a larger number of overgrowth nuclei. Third, clay/hematite coatings, considered to inhibit quartz overgrowth nucleation (Cecil and Heald, 1971; Dixon et al., 1989), are generally thinner and discontinuous in the reworked sands along the basin centre. The greatest amounts (up to 24%) of quartz overgrowths, however, were precipitated in some aeolian sands, which are richer in detrital quartz (Table 3). Some large overgrowths have locally displaced the surrounding grains, indicating that precipitation of quartz began at shallow depths. Some sandstones massively cemented by quartz (Fig. 9a) show a packing proximity index (Kahn, 1956) as low as 32–34% (Table 1). The heterogeneous packing and the limited intergranular volume of the quartz-cemented sandstones suggest, however, that quartz cementation has proceeded partially during compaction down to shallow burial. Rocks cemented near the surface by abundant early quartz overgrowths are referred to as groundwater silcretes (Smale, 1973; Summerfield, 1983; McBride, 1989), which are related to dry climatic conditions. Intraclasts of soil silcretes (cf. Thiry and Milnes, 1991), composed of chalcedony and microcrystalline quartz precipitated in the fine sediments of abandoned channel-fill, are common.

Discrete prismatic quartz occurs within intergranular (Fig. 9b) and grain-dissolution pores (Fig. 9c) commonly associated with the late burial illite (Fig. 9d) or kaolinite (Fig. 9c). This habit is reported for late burial quartz in sandstones from other basins (Thomas, 1986; De Ros, 1987; McBride, 1989), where it has precipitated in deeper burial and higher temperatures than in the Guaritas Sequence.

9.6. K-feldspar

K-feldspar occurs in trace amounts (0.1%) as thin, discontinuous overgrowths and discrete microcrystalline (2–10 μm) rhombohedral crystals. Microcrystalline K-feldspar has also replaced detrital feldspar grains in a manner similar to those described by Morad et al. (1989) in Triassic sandstones from Spain. The feldspars have a pure end-member composition characteristic of authigenic K-feldspars (Kastner and Siever, 1979; Table 4). The overgrowths are commonly covered

and replaced by coarsely crystalline calcite. Conversely, the close association of the discrete microcrystalline K-feldspar with late-burial illitic clay minerals suggests a relatively deep-burial phase.

9.7. Albite

Many of the plagioclase grains show blocky to tabular extinction, vacuolization due to the presence of numerous small fluid inclusions, and growth of euhedral crystals on the grain surface or within dissolution pores (Fig. 10a). These grains are pseudomorphs made of numerous parallel-arranged small albite crystals (cf. Morad et al., 1990). These features, along with their chemical purity (Table 3), indicate an in-situ diagenetic albitization (Gold, 1987; Milliken, 1989; Morad et al., 1990). Conversely, some vacuolized plagioclase grains are massive, show vague polysynthetic twinning, contain sericite and epidote oriented along the cleavage directions (Fig. 10b), and display An contents up to 15% (Table 3). These features indicate that the latter are grains of albite/oligoclase originated by late magmatic/deuteric, hydrothermal or low-grade metamorphic processes in the source rocks (Morad, 1988; Morad et al., 1990).

On average, diagenetic albite has replaced 4% of the detrital plagioclase in the bulk rock volume

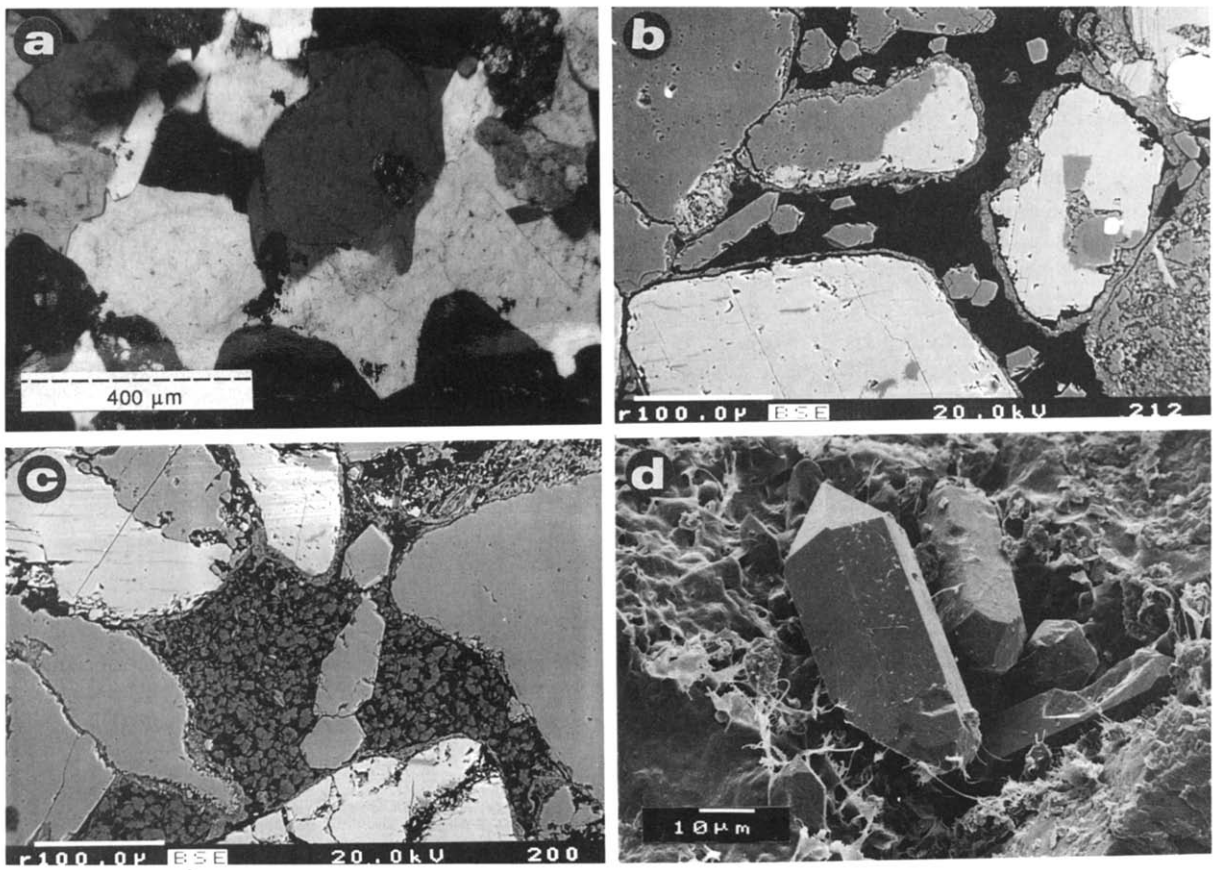

Fig. 9. (a) Micrograph (crossed polarizers) of a groundwater silcrete: aeolian sandstone massively cemented by early quartz overgrowths. (b) BSE image of discrete prismatic quartz crystals within intergranular pores lined by infiltrated clay coatings. (c) BSE image of discrete prismatic quartz crystals in pore-filling kaolinite aggregate after dissolved feldspar grain. (d) SEM photo of discrete quartz crystals on infiltrated clay-coated grain surface, bridged by late filamentous illite.

(leaving only 2%; Table 1). Among the K-feldspars, detrital microcline is fresh, whereas orthoclase/sanidine is dissolved and/or albitized (Table 4) or kaolinized. K-feldspar albitization occurred through heterogeneous replacement by very finely crystalline albite (cf. Morad, 1986, 1988; Saigal et al., 1988). Some K-feldspars were partially albitized in a complex pattern resembling "chessboard" albite (Walker, 1984). BSE analyses reveal that this pattern is due to partial replacement and not to twinning (Saigal et al., 1988). Diagenetic albitization of detrital K-feldspar (average 2.5% bulk volume), along with plagioclase albitization, corresponds to a considerable modification in the original framework composition of the sandstones. Albite occurs also as small discrete crystals associated with illitic clays (Fig. 11a).

Possible sources of Na^+ for albite authigenesis are the chloritization of intermediate volcanic rocks from the base of the sequence or from older molassic units of the basin, and the illitization/dissolution of volcanic fragments within the sequence and of detrital smectitic clays in associated mudrocks and of the clay coatings, intraclasts and pseudomatrix in the sandstones. Diagenetic albitization is intense considering the relatively low estimated maximum temperature experienced by the unit (~ 50–60°C; see Sect. 8). Although the albitization of plagioclase is recognizably enhanced at temperatures higher than 100°C (Boles, 1982), partial replacement has been

Table 4
Electron microprobe analyses and calculated formulas of detrital and authigenic feldspars and clay minerals from Guaritas sandstones

Sample	A	B	C	D	E	F	G	H	I	J	K	L
Na_2O	0.39	9.29	0.52	10.57	11.94	11.83	9.15	10.06	11.91	0.00	0.02	0.00
MgO	0.00	0.00	0.01	0.01	0.02	0.00	0.00	0.00	0.01	2.45	1.85	4.87
Al_2O_3	18.51	22.39	18.47	18.23	19.83	19.77	19.87	17.60	19.93	29.15	30.97	30.20
SiO_2	63.66	62.87	65.03	69.44	68.01	68.24	66.11	67.79	69.51	54.32	52.91	53.10
K_2O	15.94	0.16	15.66	0.09	0.01	0.02	0.08	0.00	0.04	7.83	7.69	4.85
CaO	0.00	4.04	0.00	0.10	0.15	0.42	2.28	0.18	0.01	0.37	0.58	0.35
BaO	0.51	0.00	0.09	0.00	0.00	0.00	0.00	0.00	0.00	0.00	0.00	0.12
FeO	0.00	0.05	0.00	0.10	0.00	0.03	0.01	0.00	0.08	3.05	2.14	3.81
Calc total	99.01	98.80	99.78	98.54	99.96	100.31	97.50	95.63	101.49	97.17	96.16	97.13
Ox num	8.00	8.00	8.00	8.00	8.00	8.00	8.00	8.00	8.00	22.00	22.00	22.00
Si	2.98	2.81	3.00	3.06	2.98	2.98	2.96	3.07	2.99	6.96	6.82	6.73
Al	1.02	1.18	1.01	0.95	1.02	1.02	1.05	0.94	1.01	4.40	4.71	4.51
Fe_2	0.00	0.00	0.00	0.00	0.00	0.00	0.00	0.00	0.00	0.33	0.23	0.41
Mg	0.00	0.00	0.00	0.00	0.00	0.00	0.00	0.00	0.00	0.47	0.46	0.92
Ca	0.00	0.19	0.00	0.01	0.01	0.02	0.11	0.01	0.00	0.05	0.08	0.05
Na	0.04	0.81	0.05	0.90	1.01	1.00	0.79	0.88	0.99	0.00	0.01	0.00
K	0.95	0.01	0.92	0.01	0.00	0.00	0.01	0.00	0.00	1.28	1.27	0.78
Ba	0.01	0.00	0.00	0.00	0.00	0.00	0.00	0.00	0.00	0.00	0.00	0.01
Total cat.	5.00	5.00	4.98	4.92	5.02	5.02	4.92	4.90	5.00	13.48	13.46	13.41
Ox. equiv.	8.00	8.00	8.00	8.00	8.00	8.00	8.00	8.00	8.00	22.00	22.00	22.00
Albite	3.59	79.90	4.80	98.93	99.26	97.97	87.46	99.02	99.73			
Anorthite	0.00	19.20	0.00	0.52	0.69	1.92	12.04	0.98	0.05			
Orthoclase	96.42	0.91	95.20	0.55	0.06	0.11	0.50	0.00	0.22			

(A) detrital, Ba-rich K-feldspar; (B) detrital, partially altered plagioclase; (C) discrete, microcrystalline authigenic K-feldspar; (D) and (E) albite replacing partially dissolved K-feldspar; (F) albite replacing detrital plagioclase; (G) albite replacing strongly illitized plagioclase (albitization in the source?); (H) albite outgrowth on albitized feldspar grain; (I) microcrystalline interstitial albite; (J) and (K) I/S combs in hematite–clay aggregates; (L) illitized clay coating covered by illite hairy projections.

reported at 75–100°C (Morad et al., 1990). Moreover, Saigal et al. (1988) have shown that K-feldspar albitization can occur at relatively low temperatures (~ 65°C) if a suitable sink for K^+, such as the illitization of smectite and/or neoformation of illite, is provided. Evidence from reser-

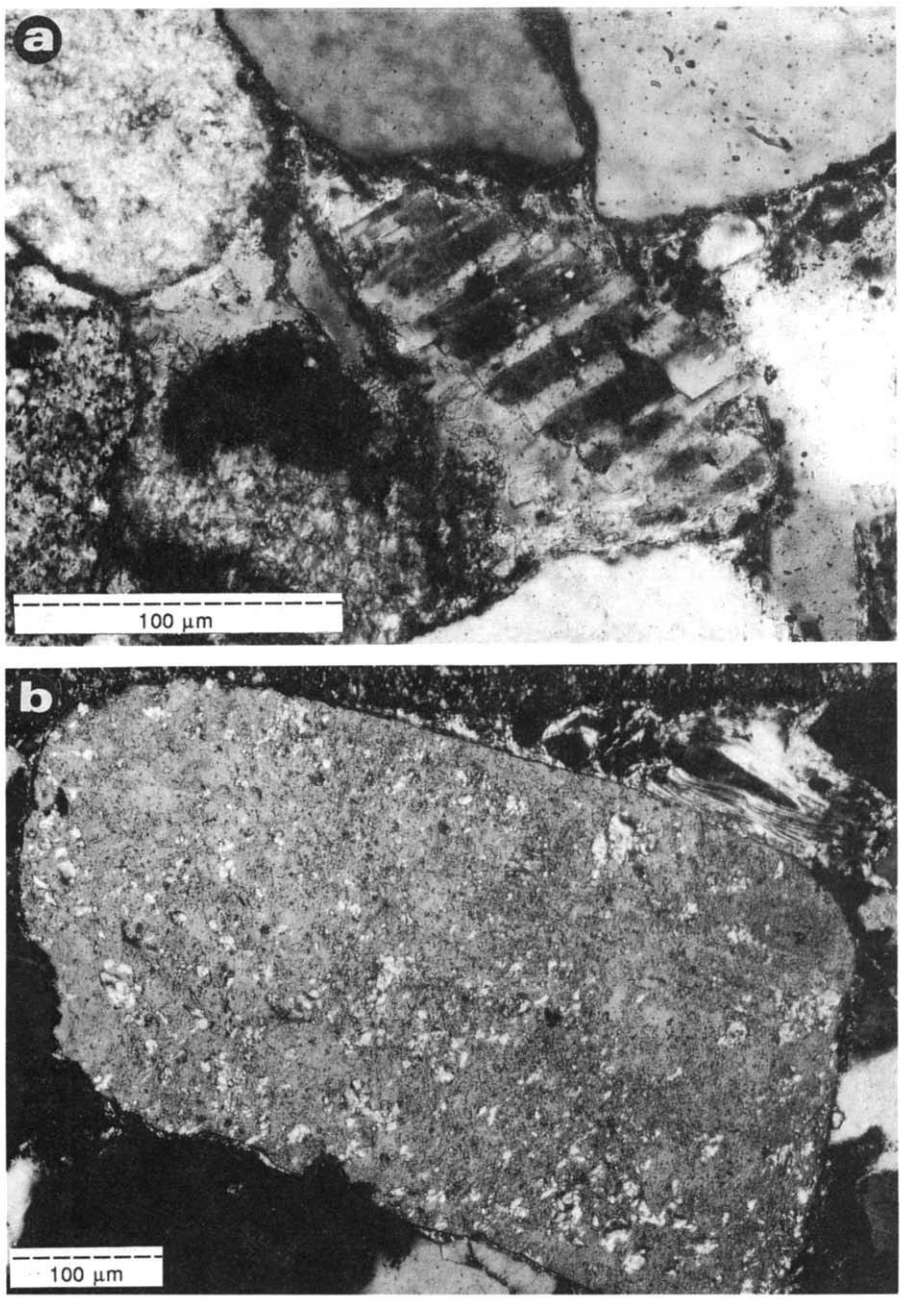

Fig. 10. (a) Micrograph (crossed polarizers) of dissolved and albitized plagioclase grain, showing typical clouded aspect, irregular twinning and crystalline terminations. (b) Micrograph (crossed polarizers) of plagioclase grain that was albitized and sericitized in the source-rock.

voir sandstones (Morad et al., 1990) and from thermodynamic calculations (Ben Baccar et al., 1993) indicate that the albitization of plagioclase occurs at a lower temperature than that for K-feldspar albitization.

9.8. Illitic clay minerals

The infiltrated clay coatings and the mud intraclasts, probably originally detrital smectites generated through semi-arid climate weathering (Keller, 1970), were transformed during burial to I/S (Figs. 6b, 6c). During burial, I/S was precipitated over smectite coatings as honeycomb-shape aggregates (Figs. 6c, 11a). During late burial, discrete illite precipitated as hair-like projections over the I/S combs, being associated with discrete quartz and albite (Figs. 9d, 11a). The illite locally bridges the pores (Fig. 9d).

Delicate "networks" of illite were generated by the progressive shrinkage of smectitic mud intraclasts and pseudomatrix during burial, due to extensive illitization (Figs. 11b, 11c). Neoformed illitic clay minerals average 1% in the sandstones (Table 1). Microprobe analysis was inaccurate because of the very small crystal size

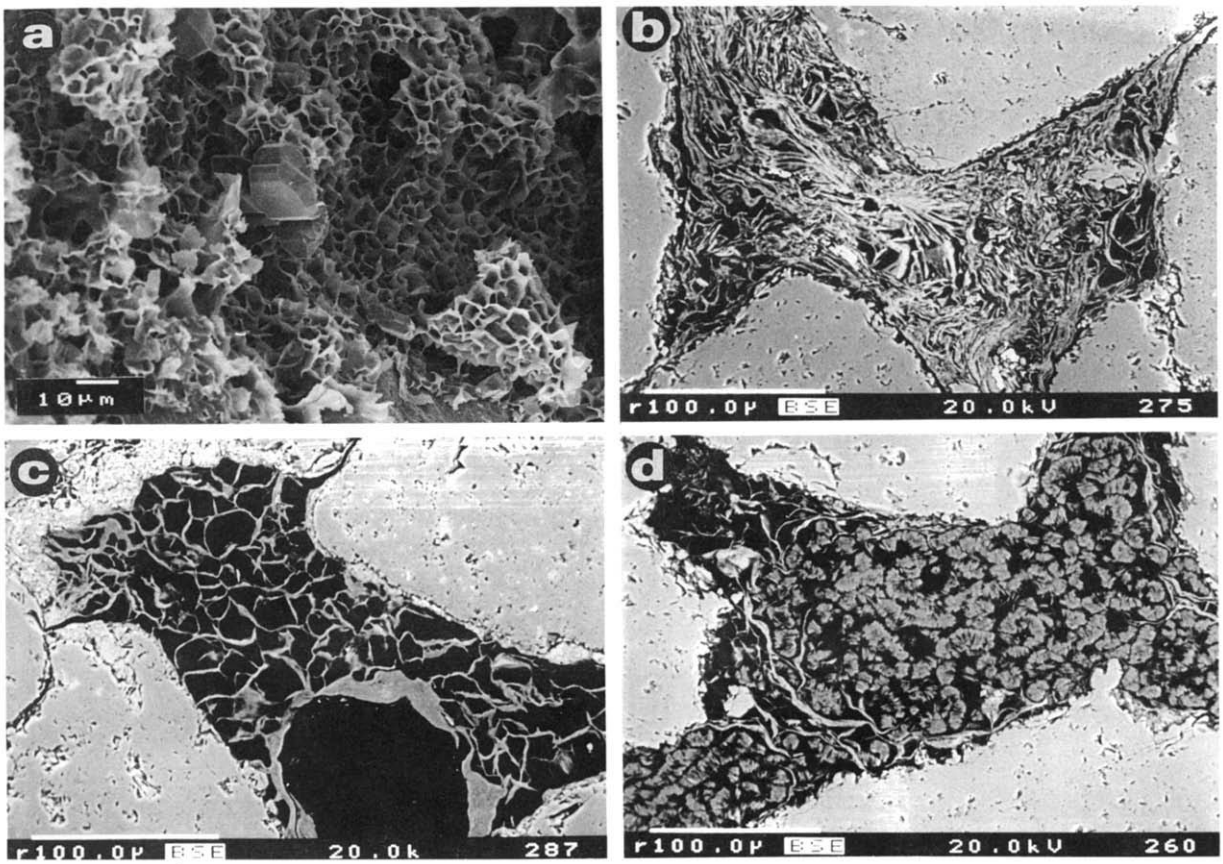

Fig. 11. (a) SEM image of microcrystalline interstitial albite associated with honeycomb-shape I/S. (b) BSE photo of pseudomatrix after mud intraclast compaction that has suffered strong shrinkage due to illitization. (c) BSE image of illite "network" generated by extreme illitization and shrinkage of smectitic pseudomatrix. (d) BSE image of kaolinite pore-filling aggregate after dissolved feldspar grain outlined by the shrinked remnants of illitized clay coatings.

of the clays. Table 4 shows examples of the composition of authigenic I/S clays. Authigenic illitic clay-minerals have the average formula:

$$K_{1.1}Ca_{0.1}(Al_{4.5}Mg_{0.6}Fe_{0.3})Si_{6.4}O_{20}(OH)_4$$

Potential sources of K^+ for illite authigenesis are the dissolution and albitization of detrital K-feldspar and the dissolution of acidic volcanic fragments.

9.9. Kaolinite

Kaolinite occurs as booklets and vermicules of pseudohexagonal crystals (total average of 1%) filling intergranular pores (up to 8%) and replacing feldspars (Fig. 11d), mud intraclasts, micaceous and volcanic rock fragments, infiltrated clays (Fig. 12a) and pseudomatrix. The authigenesis of kaolinite during burial of sandstones is usually related in the literature either to the infiltration of meteoric waters (Bjørlykke et al., 1989) or to basinal acidic fluids charged with CO_2 (Schmidt and McDonald, 1979; Franks and Forester, 1984) or with carboxylic acids (Surdam et al., 1984) derived from the thermal maturation of organic matter.

The discontinuous distribution of kaolinite along the centre of the Camaquã Basin and its absence along the margins, coupled with the association of the kaolinite with late burial illite and

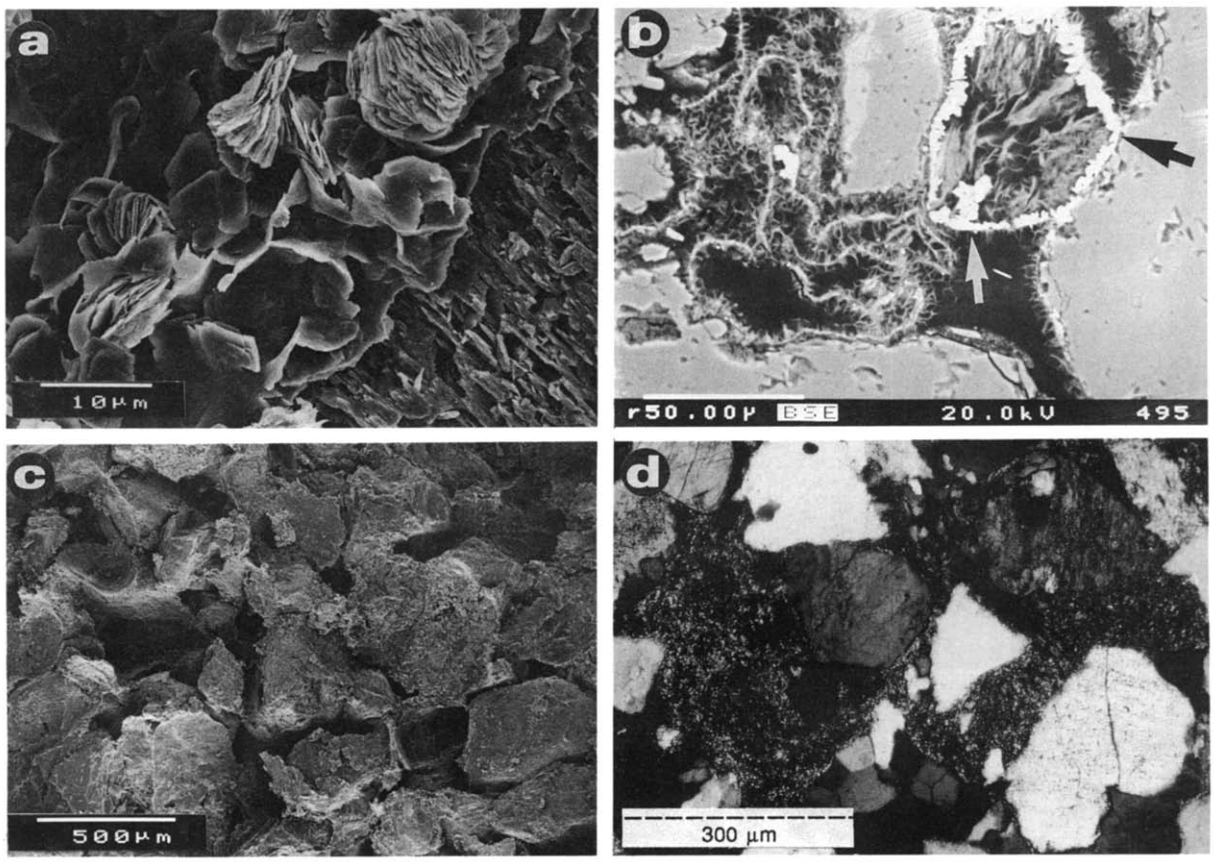

Fig. 12. (a) SEM micrograph of partially kaolinized smectitic clay coating a partially dissolved feldspar grain. (b) BSE photo of illite rimming detached clay coatings; anatase crystals rimming a clay-replaced titaniferous grain (arrows). (c) SEM photo of the textural aspect of porous, moderately compacted Guaritas sandstone. (d) Micrograph (crossed polarizers) of pseudomatrix from the compaction of micaceous metamorphic rock fragments and mud intraclasts.

discrete quartz attest against a meteoric origin. Because there are no reported organic-rich shales in the basin from which CO_2 could be generated or carboxylic acids, the origin of the fluids that have precipitated the kaolinite and dissolved the feldspars (Fig. 12a), calcite, hematite and pseudomatrix during burial is enigmatic.

9.10. Anatase

Finely crystalline anatase (average 0.3%) was precipitated as a result of the near-surface alteration of detrital sphene, ilmenite, biotite and intermediate volcanic lithoclasts. Microcrystalline anatase occurs as residual rims around these titaniferous grains (cf. Morad and AlDahan, 1986) that underwent dissolution or replacement by clay minerals, hematite or calcite (Fig. 12b), or randomly scattered in altered volcanic fragments. Euhedral and well-developed crystals of anatase are associated with heavy-mineral grain remnants, representing probably a burial recrystallization of early diagenetic microcrystalline Ti oxides.

9.11. Minor phases

Other minor late burial phases include microcrystalline chlorite, pyrite and sphene, which occur in trace amounts, usually replacing or rimming mud intraclasts/pseudomatrix, intermediate volcanic rock fragments and biotite.

10. Compaction and porosity

The Guaritas Sequence shows a lower degree of compaction and a higher remaining intergranular porosity (Fig. 12c) than would be expected for Cambro–Ordovician molasses rich in ductile lithic fragments. The average packing proximity index (Kahn, 1956) of 56% would better correspond to Mesozoic or Tertiary sandstones than to Eo–Palaeozoic molasses. Considering the detrital composition and age, the average intergranular volume is relatively high (19%). Conversely, sediments devoid of early cements show intensive compaction, as evidenced by the deformation of ductile mud intraclasts, micaceous low-grade metamorphic (Fig. 12d) and altered volcanic rock fragments into pseudomatrix (0 to 9%; average 1.5% of sandstones; up to 20% in intraclastic conglomerates). Compaction has also caused fracturing of feldspar and quartz grains. Chemical compaction, evidenced by pressure dissolution along the intergranular contacts of the quartz grains and some of the volcanic lithoclasts, generated concavo–convex and sutured contacts. Remaining primary intergranular porosity averages 3% of bulk Guaritas sandstones. Grain-dissolution porosity averages 2% and total macroporosity averages 6% (Table 1).

The plot of cement percentage versus intergranular volume percentage of the Guaritas sandstones (Fig. 13; Houseknecht, 1987) indicates that compaction was more important than cementation in porosity reduction, and that the samples with higher intergranular volume have consistently higher volume of cement. This distribution pattern and the low average macroporosity (6%; Table 1) suggest that early cementation by quartz,

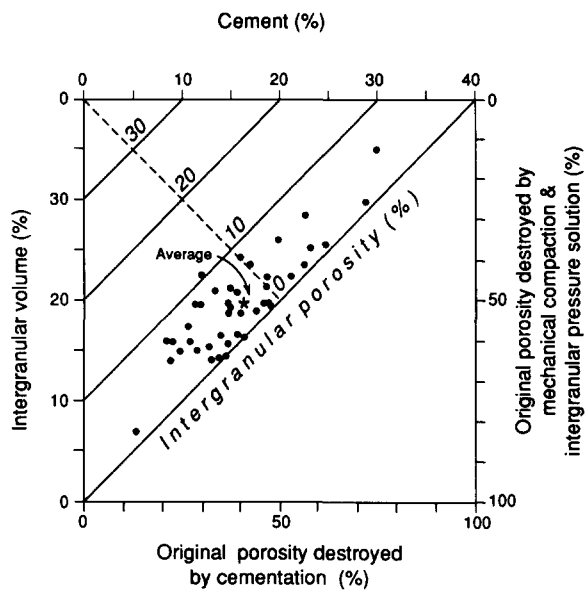

Fig. 13. Diagram of cement (%) versus intergranular volume (%) (Houseknecht, 1987) of 42 Guaritas sandstones, showing that compaction was slightly more important than cementation in porosity reduction, and that higher intergranular volumes correspond to larger amounts of early cements.

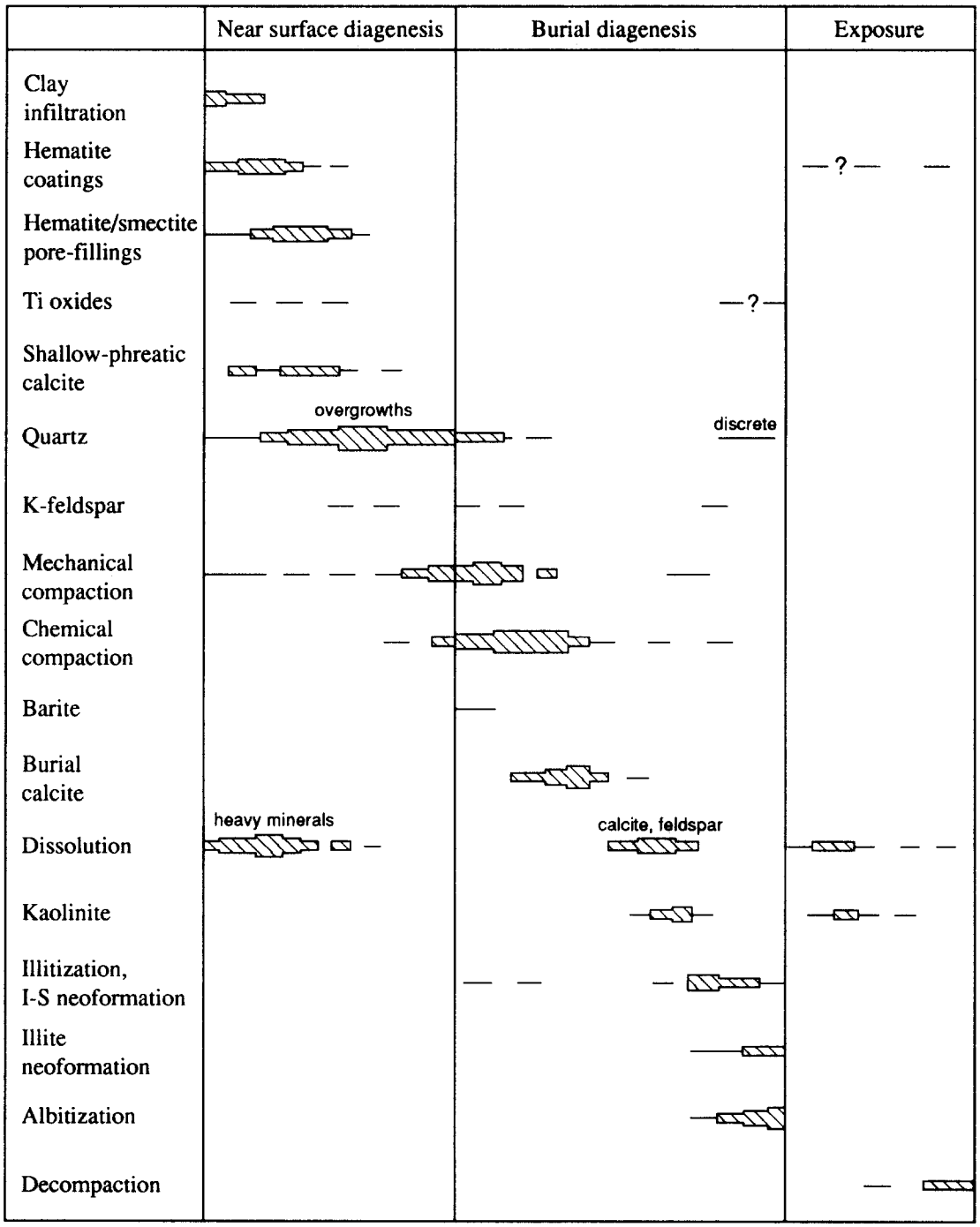

Fig. 14. Paragenetic sequence of diagenetic processes and products in Guaritas sandstones. Thickness of the bars correspond to the relative importance of each phase.

calcite, hematite and clays limited compaction through the stabilization of the ductile framework of the molasses. The moderate maximum burial depth is an additional reason for the limited compaction.

11. Diagenetic patterns

The full paragenetic sequence in the Guaritas sandstones is schematically represented in Fig. 14. Sandstones with some specific detrital compositions do not show this complete sequence due to mutually exclusive relationships between the processes. The main controls on the diagenetic evolution were the composition and texture of detrital grains and the amount of early cements. Seven main diagenetic evolution pathways were identified and assigned to specific detrital compositional variations or diagenetic processes:

(A) The dominant evolutionary pathway was developed in the modal lithic arkose/feldspathic litharenite ("feldspatholithic") detrital composition (branch "A" in Fig. 15). In most of these sands, the small amounts of detrital quartz, and clay–hematite coatings, limited quartz cementation to a small volume of overgrowths, yet enough (> 1–2%) to help protect the framework from strong compaction. Remaining permeability and porosity were high enough to allow some precipitation of burial calcite, dissolution, and late illitic clays, quartz and feldspar albitization. The final products of this evolution pathway are sandstones still relatively porous and with a complex authigenic mineralogy.

(B) Similar sands with trace or no early quartz cementation suffered a stronger mechanical and chemical compaction, which resulted in a drastic reduction of permeability and porosity, resulting in tight sandstones. Consequently, further diagenetic changes were limited (branch "B" in Fig. 15).

(C) Where burial calcite cementation was abundant enough to obliterate intergranular porosity, the diagenetic evolution was interrupted, as shown in branch "C" in Fig. 15.

(D) Locally, intense burial dissolution and kaolinization of feldspars, rock fragments and mud intraclasts occurred, resulting in microporous sandstones (branch "D" in Fig. 15).

Sands with original detrital compositions deviating from the modal "feldspatholithic" composition fall into three major groups with different diagenetic evolution pathways (Fig. 16).

(E) Sands with abundant (> 5–10%) chemically unstable grains (pyroxenes, amphiboles, garnets, epidotes, staurolite and vitric volcanic rock fragments), followed the pathway "E" (Fig. 16). The alteration of these grains under the oxidizing near-surface conditions generated abundant pore-filling hematite and smectitic clays, thereby limiting compaction and further diagenetic changes, except for scarce calcite precipitation, dissolution and clay illitization.

(F) Sands with abundant ductile grains suffered early and intense mechanical compaction (cf. Pittman and Larese, 1991; Lundegard, 1992), and consequently the inhibition of burial diagenetic changes (pathway "F", Fig. 16).

(G) Reworked aeolian and fluvial sands occurring in the basin centre, which are most enriched in quartz, and mechanically resistant rhyolite fragments have been extensively cemented by quartz overgrowths, consequently resulting in the inhibition of compaction and of burial changes (pathway "G", Fig. 16).

12. Effects of diagenetic changes on classification and provenance interpretation

The present framework compositions of Guaritas sandstones range from litharenites to arkoses (classification of Folk, 1968; Fig. 3), whereas the reconstructed original compositions cluster mostly in the lithic arkose and arkose fields (Fig. 3). The shift is related to the preferential replacement and dissolution of the feldspars in relation to the lithoclasts and quartz. It is important to remember here that all granitic/gneissic rock fragments are plotted as F in Folk's classification.

The original amount of low-rank metamorphic rock fragments is underestimated, because there are no unequivocal criteria to differentiate pseudomatrix generated by strong compaction of slate and phyllite lithoclasts from pseudomatrix de-

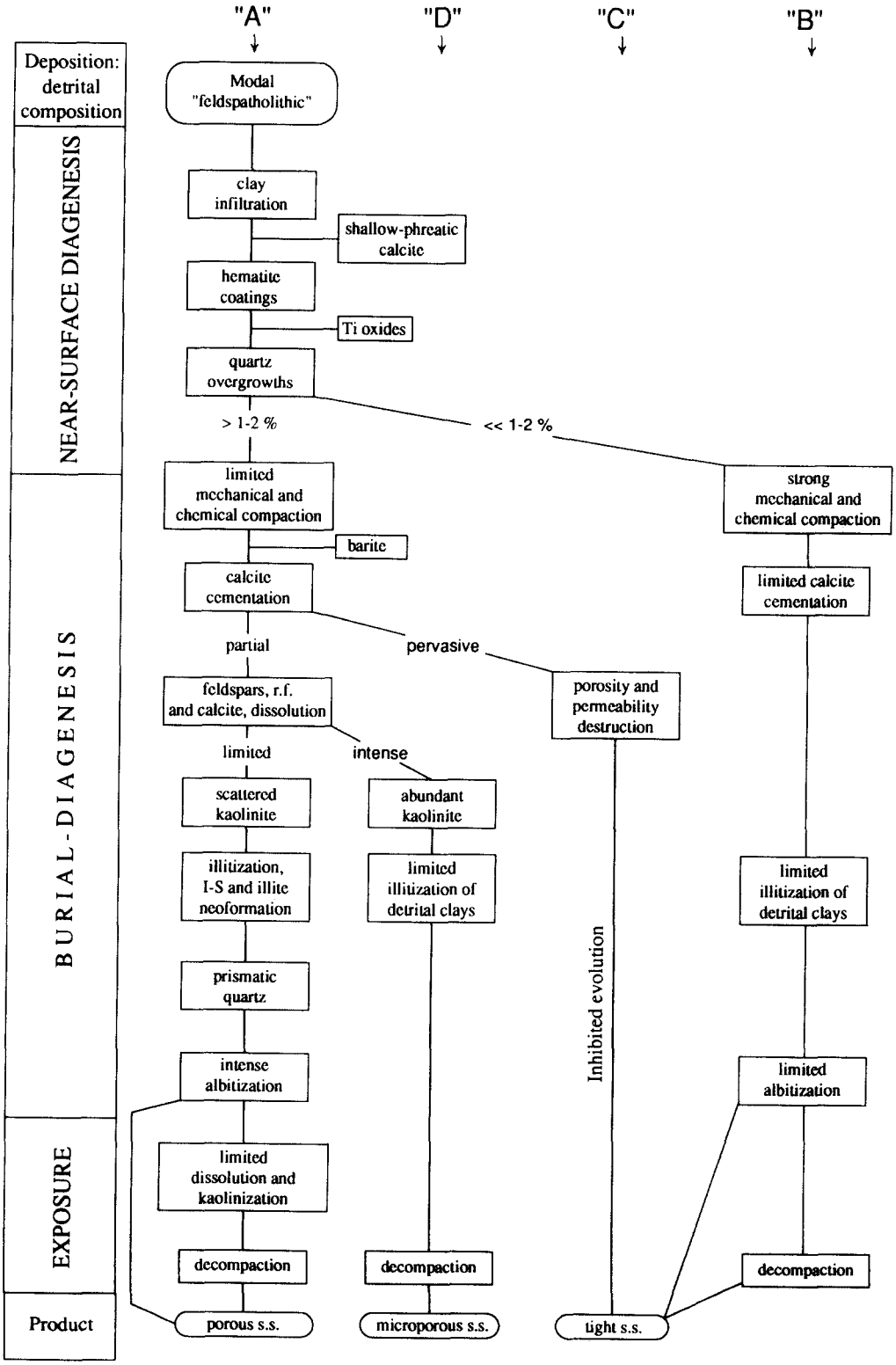

Fig. 15. Main diagenetic evolution pathways of the Guaritas Sequence sandstones with the modal lithic arkose/feldspathic litharenite ("feldspatholithic") detrital composition. Explanation in the text.

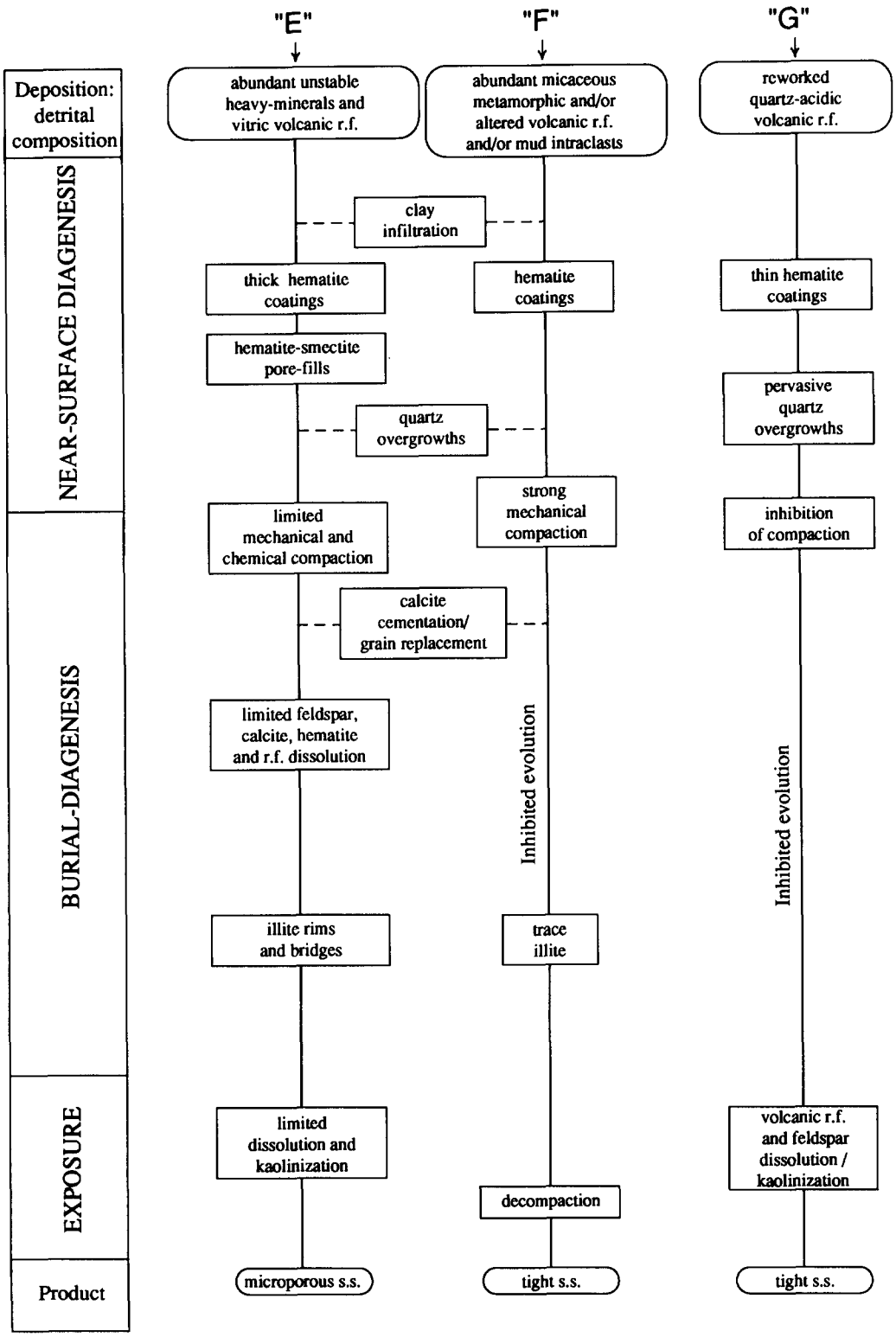

Fig. 16. Diagenetic evolution pathways of the three main groups of detrital compositions of Guaritas sandstones that deviate from the "feldspatholithic" mode. Explanation in the text.

rived from the common mud intraclasts. To avoid this confusion, pseudomatrix was not considered in the reconstructions.

The characterization of the tectonic setting of sandstones and their source areas through plots of detrital modes is a commonly utilized procedure in provenance analysis (Dickinson and Suczec, 1979; Dickinson et al., 1983; Dickinson, 1985; Zuffa, 1985). However, most work dealing with provenance interpretations based on these

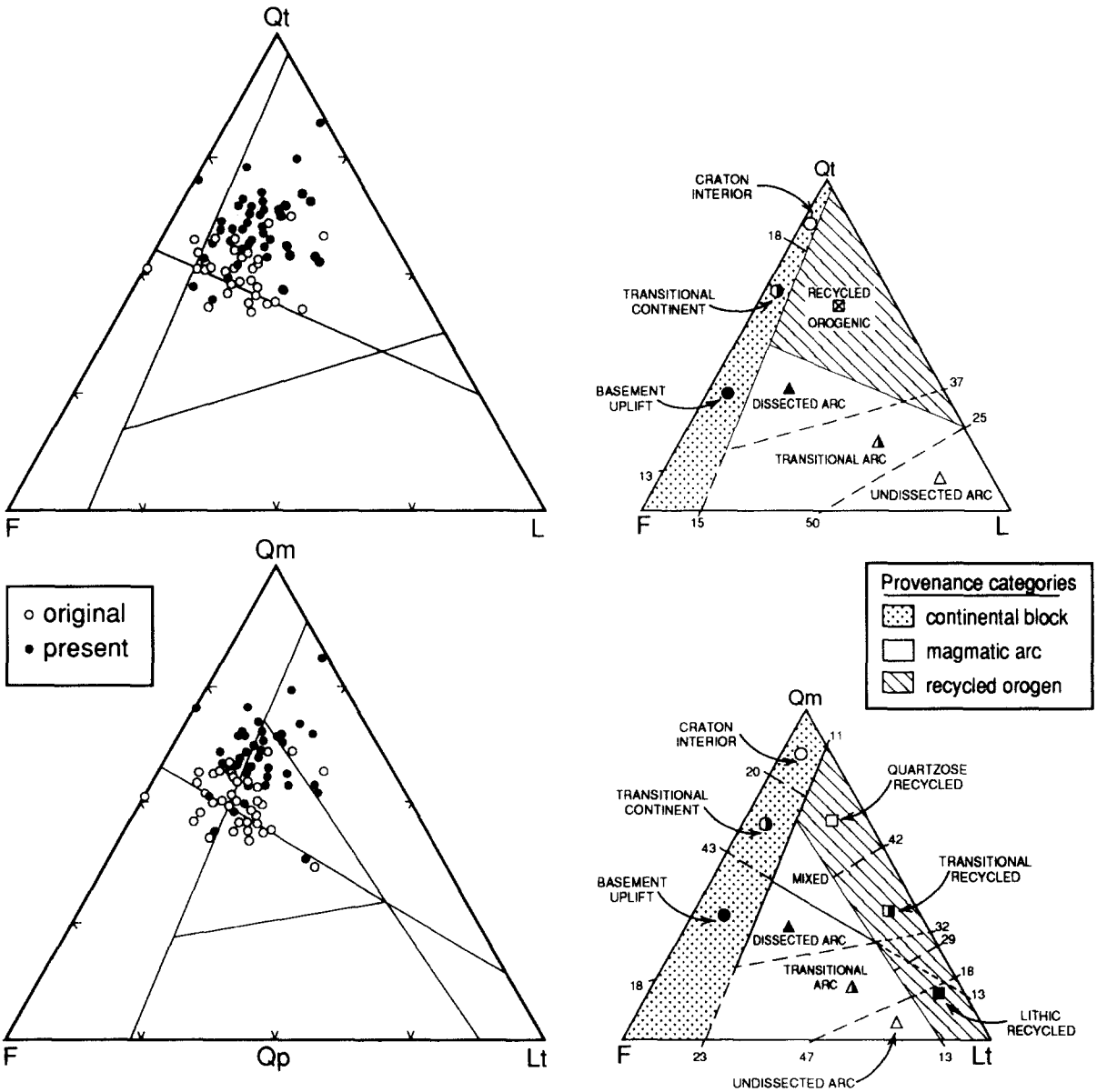

Fig. 17. Compositional plots of the tectonic setting of provenance of Guaritas sandstones. Compositional fields after Dickinson et al. (1983). *Qt* = total quartzose grains; *F* = total feldspar grains; *L* = total unstable lithic fragments; *Qm* = monocrystalline quartz (> 0.0625 mm); *Qp* = polycrystalline quartz (or chalcedony); *Lt* = L + Qp.

plots do not take into consideration the diagenetic changes of framework composition. Due to the widespread dissolution and replacement of feldspar and rock fragments in Guaritas sandstones, the framework composition was changed considerably to shift the classification of many samples (Fig. 3). Accordingly, the plotting of Guaritas sandstones on the Qt–F–L tectonic provenance diagram of Dickinson et al. (1983) (Fig. 17) shows an originally mixed arc–recycled orogenic source, with some contribution of transitional basement uplift. This corresponds well to the scenario of a narrow molassic basin between the metamorphic–magmatic terrains of the Caçapava do Sul and Santana da Boa Vista highs, with older (mostly in the Lavras do Sul region) and penecontemporaneous intrabasinal volcanism (Fig. 1). The selective replacement and dissolution of feldspars generated the present compositions, concentrated in the recycled orogenic field, thereby masking the arc contribution (Fig. 17). Similarly, diagenesis has caused a shift in the Qm–F–Lt plot (Dickinson et al., 1983) from an original mixture of dissected arc/mixed-transitional continental block/basement uplift towards the quartzose recycled orogenic field. This shift is due to the destruction of feldspars and volcanic rock fragments (Fig. 17). The changes on the provenance characterization of Guaritas sandstones show that diagenetic modifications of original detrital composition must always be considered in order to achieve reliable provenance interpretations (McBride, 1985).

13. Conclusions

In this study, the relationships between detrital composition and diagenesis of a continental molassic sequence have been identified. Seven different pathways of paragenetic evolution were recognized and assigned to specific detrital compositions and resulting diagenetic processes. The original framework composition and tectonic provenance setting were reconstructed. The results achieved in the systematic petrographic analysis of the Guaritas Sequence indicate the efficiency of this method for the development of realistic diagenetic models comprising multiple evolutive pathways, and for the provenance analysis of ancient sandstones.

The Guaritas Sequence represents a typical example of molassic sediments with a complex detrital composition that have evolved through an intense near-surface diagenesis under semi-arid continental conditions to shallow burial diagenesis. The limited burial and the partial early cementation by hematite, smectitic clays, quartz and calcite supported the framework against intense compaction, allowing the preservation of intergranular porosity and the authigenesis of calcite, kaolinite, illite, and albite during burial. Conversely, sands without partial near-surface cementation and/or with large amounts of ductile rock fragments and intraclasts suffered early and intense compaction, porosity destruction and inhibition of further diagenetic processes. The alteration of chemically unstable heavy-minerals and volcanic grains resulted in abundant near-surface cementation by hematite–clay aggregates. Massive quartz overgrowth cementation occurred in reworked more quarzose aeolian or basin-centre fluvial sands. Locally, abundant calcite cementation has obliterated the pores of arkosic sands. Burial diagenesis was inhibited where these early cementation processes were pervasive.

The selective destruction of detrital feldspars and volcanic lithoclasts during diagenesis resulted in significant modifications of the original compositional classification and tectonic provenance characterization of Guaritas molasses, which was reconstructed by a detailed petrographic analysis. This study illustrates the importance of considering the diagenetic changes in original detrital compositions in order to achieve trustful provenance interpretations.

Acknowledgements

L.F.D.R. and P.S.G.P. acknowledge the scholarships granted by Brazil National Council of Research, CNPq (grants 200465/92.9-GL and 204072/89.1-GL). S.M. thanks the Swedish Natural Science Research Council, NFR, for financial research support. L.F.D.R. thanks Rio Grande

do Sul State Foundation for Research Support (FAPERGS), for funding field work and initial analyses, and the help from Dr. A.J.V. Garcia and the Vale dos Sinos University (Unisinos). P.S.G.P. thanks the field support of CNPq (grant 413321188-6), Companhia de Pesquisas de Recursos Minerais (CPRM) and Unisinos. Revisions by Drs. E.F. McBride, H. Füchtbauer and K.A.W. Crook helped to substantially improve the manuscript. Suggestions of Dr. G.G. Zuffa were very useful. A.A.S. da Rosa and K. Goldberg were extremely helpful during initial data acquisition and organization. Thin sections were prepared at the Federal University of Rio Grande do Sul (UFRGS). We thank C. Wernström for drafting the figures, I.S. Al-Aasm for the isotope analyses, C. Bäck and B. Giös for photo work, and H. Harryson for aiding with the microprobe analyses.

References

Almeida, D.P.M., Paim, P.S.G. and Vieira, N., Jr., 1992. Petrologia do vulcanismo Eo–Paleozóico das Bacias do Camaquã e Santa Bárbara, RS. 1° Workshop sobre as Bacias Molássicas Brasilianas, Bol. Res. Expand., pp. 16–22.

Almeida, F.F.M., 1971. Geochronological division of the Precambrian of South America. Rev. Bras. Geocienc., 1: 13–21.

Beckel, J., 1990. Metalogenia del Cu, Pb y Zn en la Cuenca de Camaquã durante el Ciclo Orogenico Brasiliano–Rio Grande del Sur (Brasil). Umpublished PhD Thesis, University of Salamanca, 274 pp.

Beckel, J., 1992. Evolução geotectônica da Bacia do Camaquã, RS—Proposta de classificação dentro de um conceito mobilista. 1° Workshop sobre as Bacias Molássicas Brasilianas, Bol. Res. Expand., pp. 1–5.

Becker, M.R. and Fernandes, L.A.D., 1982. Caracterização faciológica de uma sequência vulcano-sedimentar Eo–Paleozóica na Folha Passo do Tigre (RS). Acta Geol. Leopoldensia, 13(6): 287–321.

Ben Baccar, M., Fritz, B. and Madé, B., 1993. Diagenetic albitization of K-feldspar and plagioclase in sandstone reservoirs: thermodynamic and kinetic modelling. J. Sediment. Petrol., 63(6): 1100–1109.

Bjørlykke, K., Ramm, M. and Saigal, G.C., 1989. Sandstone diagenesis and porosity modification during basin evolution. Geol. Rundsch., 78(1): 243–268.

Boles, J.R., 1982. Active albitization of plagioclase, Gulf Coast Tertiary. Am. J. Sci., 282: 165–180.

Bonhome, M.E. and Ribeiro, M.J., 1983. Datações K/Ar das argilas associadas à mineralização de cobre da Mina do Camaquã e suas encaixantes. 1° Simpósio Sulbrasileiro de Geologia, Atas, pp. 82–88.

Brito Neves, B.B. and Cordani, U.G., 1991. Tectonic evolution of South America during the Late Proterozoic. Precambrian Res., 53: 23–40.

Cecil, C.B. and Heald, M.T., 1971. Experimental investigation of the effects of grain coatings on quartz growth. J. Sediment. Petrol., 41: 582–584.

Craig, H., 1957. Isotopic standards for carbon and oxygen correction factors for mass spectrometric analysis of carbon dioxide. Geochim. Cosmochim. Acta, 12: 133–149.

De Ros, L.F., 1987. Petrologia e caracteristicas de reservatório de Formação Sergi (Jurássico) no campo de Sesmaria, Bacia do Recôncavo, Brasil. Ciência—Técnica—Petróleo, Seção: Exploração de Petróleo 19, PETROBRAS/CENPES, Rio de Janeiro, 107 pp.

Dickinson, W.R., 1985. Interpreting provenance relations from detrital modes of sandstones. In: G.G. Zuffa (Editor), Provenance of Arenites. NATO–ASI Series C, 148, D. Reidel, Dordrecht, pp. 333–361.

Dickinson, W.R. and Suczec, C.A., 1979. Plate tectonics and sandstone composition. Am. Assoc. Pet. Geol. Bull., 63: 2164–2182.

Dickinson, W.R., Beard, L.S., Bankenridge, G.R., Erjavec, J.L., Ferguson, R.C., Inman, K.F., Knepp, R.A., Lindberg, F.A. and Ryberg, P.T., 1983. Provenance of North American Phanerozoic sandstones in relation to tectonic setting. Geol. Soc. Am. Bull., 94: 222–235.

Dixon, S.A., Summers, D.M. and Surdam, R.C., 1989. Diagenesis and preservation of porosity in Norphlet Formation (Upper Jurassic), Southern Alabama. Am. Assoc. Pet. Geol. Bull., 73: 707–728.

Dutta, P.K. and Suttner, L.J., 1986. Alluvial sandstone composition and paleoclimate, II. Authigenic mineralogy. J. Sediment. Petrol., 56(3): 346–358.

Folk, R.L., 1968. Petrology of Sedimentary Rocks. Hemphill, Austin, Texas, 107 pp.

Fragoso-Cesar, A.R.S., 1980. O Cráton do Rio de La Plata e o Cinturão Dom Feliciano no Escudo Uruguaio-Sul-rio-grandense. Congr. Brasil. Geol., 31, Camboriú, Anais, 5: 2879–2892.

Fragoso-Cesar, A.R.S., Wernick, E. and Soliani, E., Jr., 1982. Evolução geotectônica do Cinturão Dom Feliciano—uma contribuição através da aplicação do modelo de tectônica de placas. Congr. Brasil. Geol., 32, Salvador, Anais, 1: 13–23.

Fragoso-Cesar, A.R.S., Lavina, E.L., Paim, P.S.G. and Faccini, U.F., 1984. A Antefossa Molássica do Cinturão Dom Feliciano no Escudo do Rio Grande do Sul. Congr. Brasil. Geol., 33, Rio de Janeiro, Anais, pp. 3272–3283.

Fragoso-Cesar, A.R.S., Machado, R., Sayeg, H. and Fambrini, G.L., 1992. Bacias orogênicas do ciclo Brasiliano no Rio Grande do Sul e Uruguai. 1° Workshop sobre as Bacias Molássicas Brasilianas, 1, Bol. Res. Expand., pp. 47–53.

Franks, S.G. and Forester, R.W., 1984. Relationships among secondary porosity, pore fluid chemistry and carbon diox-

ide, Texas Gulf Coast. In: D.A. McDonald and R.C. Surdam (Editors), Clastic Diagenesis. Am. Assoc. Pet. Geol. Mem., 37: 63–79.

Füchtbauer, H., 1974. Sediments and Sedimentary Rocks, 1. Sedimentary Petrology, Part II. Schweizerbart, Stuttgart, 464 pp.

Gold, P.B., 1987. Textures and geochemistry of authigenic albite from Miocene sandstones, Louisiana Gulf Coast. J. Sediment. Petrol., 57: 353–362.

Haug, E., 1900. Les géosynclinaux et les aires continentales: contribution à l'étude des transgressions et des regressions marines. Bull. Soc. Geól. Fr., 3(28): 617–711.

Houseknecht, D.W., 1987. Assessing the relative importance of compaction processes and cementation to reduction of porosity in sandstones. Am. Assoc. Pet. Geol. Bull., 71: 633–642.

Jost, H., 1984. Sedimentação e vulcanismo durante o ciclo Brasiliano no Rio Grande do Sul: uma revisão. Congr. Brasil. Geol., 33, Rio de Janeiro, Anais, pp. 3241–3257.

Kahn, J.S., 1956. The analysis and distribution of the properties of packing in sand-size sediments, 1. On the measurement of packing in sandstones. J. Geol., 64: 385–395.

Kastner, M. and Siever, R., 1979. Low temperature feldspars in sedimentary rocks. Am. J. Sci., 279: 435–479.

Keller, W.D., 1970. Environmental aspects of clay minerals. J. Sediment. Petrol., 40: 788–813.

Keller, W.D., Reynolds, R.C. and Inoue, A., 1986. Morphology of clay minerals in the smectite-to-illite conversion series by scanning electron microscopy. Clays Clay Miner, 34(2): 187–197.

Lavina, E.L., Faccini, U.F., Paim, P.S.G. and Fragoso Cesar, A.R., 1985. Ambientes de sedimentação da Bacia do Camaquã, Eo–Paleozóico do Rio Grande do Sul. Acta Geol. Leopoldensia, 21: 185–227.

Leeder, M.R., 1975. Pedogenic carbonates and flood sediment accretion rates: a quantitative model for alluvial arid-zone lithofacies. Geol. Mag., 112: 257–270.

Lundegard, P.D., 1992. Sandstone porosity loss—a "big picture" view of the importance of compaction. J. Sediment. Petrol., 62(2): 250–260.

Matlack, K.S., Houseknecht, D.W. and Applin, K.R., 1989. Emplacement of clay into sand by infiltration. J. Sediment. Petrol., 59: 77–87.

Maurer, H., Gerber, M.E. and Nabholz, W.K., 1982. Sedimentpetrographie und lithostratigraphie der Molasse im Einzugsgebiet der Langete (Aarwangen-Naupf, Oberaargau). Eclogae Geol. Helv., 75(2): 381–413.

McBride, E.F., 1985. Diagenetic processes that affect provenance determinations in sandstone. In: G.G. Zuffa (Editor), Provenance of Arenites. NATO–ASI Series C, 148, D. Reidel, Dordrecht, pp. 95–113.

McBride, E.F., 1989. Quartz cement in sandstones: a review. Earth Sci. Rev., 26(2): 69–112.

Miall, A.D., 1978. Lithofacies types and vertical profile models in braided river deposits: a summary. In: A.D. Miall (Editor), Fluvial Sedimentology. Can. Soc. Pet. Geol. Mem., 5: 597–604.

Milliken, K.L., 1989. Petrography and composition of authigenic feldspars, Oligocene Frio Sequence, South Texas. J. Sediment. Petrol., 59(3): 361–374.

Morad, S., 1983. Diagenesis and geochemistry of the Visingsö Group (Upper Proterozoic), southern Sweden: a clue to the origin of colour differentiation. J. Sediment. Petrol., 53: 51–65.

Morad, S., 1986. Albitization of K-feldspar grains in Proterozoic arkoses and greywackes from southern Sweden. Neues Jahrb. Miner. Monatsh., 4: 145–156.

Morad, S., 1988. Albitized microcline grains of post-depositional and probable detrital origins in Brøttum Formation sandstones (Upper Proterozoic), Sparagmite Region of southern Norway. Geol. Mag., 125(3): 229–239.

Morad, S. and AlDahan, A.A., 1986. Alteration of detrital Fe–Ti oxides in sedimentary rocks. Geol. Soc. Am. Bull., 97: 567–578.

Morad, S., Marfil, R. and De La Peña, J.A., 1989. Diagenetic K-feldspar pseudomorphs in the Triassic Buntsandstein sandstones of the Iberian Range, Spain. Sedimentology, 36: 635–650.

Morad, S., Bergman M., Knarud, R. and Nystuen J.P., 1990. Albitization of detrital plagioclase in Triassic reservoir sandstones from the Snorre field, Norwegian North Sea. J. Sediment. Petrol., 60(3): 411–425.

Moraes, M.A.S. and De Ros, L.F., 1990. Infiltrated clays in fluvial Jurassic sandstones of Recôncavo Basin, Northeastern Brazil. J. Sediment. Petrol., 60(6): 809–819.

Paim, P.S.G., 1992. Alluvial paleogeography of Guaritas depositional sequence (Cambro–Ordovician of southern Brazil). 1° Workshop sobre as Bacias Molássicas Brasilianas, Bol. Res. Expand., pp. 113–119.

Paim, P.S.G., in prep. Fluvial palaeogeography of the Guaritas Depositional Sequence of southern Brazil. Int. Assoc. Sedimentol. Spec. Publ.

Paim, P.S.G. and De Ros, L.F., in prep. Architectural elements of a trunk braid river system in a semi-arid climate: an example from the Cambro–Ordovician Guaritas Sequence (Brazil).

Pittman, E.D. and Larese, R.E., 1991. Compaction of lithic sands: experimental results and applications. Am. Assoc. Pet. Geol. Bull., 75(8): 1279–1299.

Platt, N.H., 1992. Fresh-water carbonates from the Lower Freshwater Molasse (Oligocene, western Switzerland): sedimentology and stable isotopes. Sediment. Geol., 78: 661–669.

Plymate, T.G. and Suttner, L.J., 1983. Evaluation of optical and X-ray techniques for detecting source-rock-controlled variation in detrital potassium feldspar. J. Sediment. Petrol., 53(2): 509–519.

Porada, H., 1979. The Damara–Ribeira Orogen of the Panafrican–Brasiliano Cycle in Namibia (Southwest Africa) and Brazil as interpreted in terms of continental collision. Tectonophysics, 57: 237–265.

Porada, H., 1989. Pan-African rifting and orogenesis in Equatorial Africa and Eastern Brazil. Precambrian Res., 44: 103–136.

Rust, B.R. and Koster, E.H., 1984. Coarse alluvial deposits. In: R.G. Walker (Editor), Facies Models. Geosci. Can., Reprint Ser., 1: 71–89.

Saigal, G.C., Morad, S., Bjørlykke, K., Egeberg, P.K. and Aagaard, P., 1988. Diagenic albitization of detrital K-feldspars in Jurassic, Lower Cretaceous, and Tertiary clastic reservoirs from offshore Norway, I. Textures and origin. J. Sediment. Petrol., 58: 1003–1013.

Schmidt, V. and McDonald, D.A., 1979. The role of secondary porosity in the course of sandstone diagenesis. In: P.A. Scholle and P.R. Schluger (Editors), Aspects of Diagenesis. Soc. Econ. Paleontol. Mineral. Spec. Publ., 26: 175–207.

Schwab, F.L., 1986. Sedimentary 'signatures' of foreland basin assemblages: real or counterfeit? In: P.A. Allen and P. Homewood (Editors), Foreland Basins. Int. Assoc. Sedimentol., Spec. Publ., 8: 395–410.

Scotese, C.R. and Barret, S.F., 1990. Gondwana's movement over the South Pole during the Paleozoic: evidence from lithological indicators of climate. In: W.S. McKerrow and C.R. Scotese (Editors), Palaeozoic Palaeogeography and Biogeography. Geol. Soc. London Mem., 12: 75–85.

Smale, D., 1973. Silcretes and associated silica diagenesis in southern Africa and Australia. J. Sediment. Petrol., 43(4): 1077–1089.

Soliani, E., Jr., Fragoso-Cesar, A.R.S., Teixeira, W. and Kawashita, K., 1984. Panorama geocronológico da porção meridional do Escudo Atlântico. XXXIII Congresso Brasileiro de Geologia, Rio de Janeiro, RJ, SBG, Anais, pp. 2435–2449.

Strong, G.E. and Milodowsky, A.E., 1987. Aspects of the diagenesis of the Sherwood Sandstones of the Wessex Basin and their influence on reservoir characteristics. In: J.D. Marshall (Editor), Diagenesis of Sedimentary Sequences. Geol. Soc. Spec. Publ., 36: 325–337.

Studer, B., 1825. Beyträge zu einer Monographie der Molasse. C.A. Jenni, Bern, 427 pp.

Suchecki, R.K., Hubert, J.F. and De Wet, C.C.B., 1988. Isotopic imprint of climate and hydrogeochemistry on terrestrial strata of the Triassic–Jurassic Hartford and Fundy basins. J. Sediment. Petrol., 58: 801–811.

Summerfield, M.A., 1983. Petrography and diagenesis of silcrete from the Kalahari basin and Cape Coastal zone, southern Africa. J. Sediment. Petrol., 53(3): 895–909.

Surdam, R.C, Boese, S.W. and Crossey, L.J., 1984. The chemistry of secondary porosity. In: D.A. McDonald and R.C. Surdam (Editors), Clastic Diagenesis. Am. Assoc. Pet. Geol. Mem., 37: 127–149.

Suttner, L.J. and Basu, A., 1977. Structural state of detrital feldspars. Sedimentology, 26: 63–74.

Suttner, L.J. and Dutta, P.K., 1986. Alluvial sandstone composition and paleoclimate, I. Framework mineralogy. J. Sediment. Petrol., 56(3): 329–345.

Thiry, M. and Milnes, A.R., 1991. Pedogenic and groundwater silcretes at Stuart Creek opal field, South Australia. J. Sediment. Petrol., 61(1): 111–127.

Thomas, M., 1986. Diagenetic sequences and K/Ar dating in Jurassic sandstones, Central Viking Graben: effects on reservoir properties. Clay Miner., 21: 695–710.

Turner, P. and Archer, R., 1977. The role of biotite in the diagenesis of red beds from the Devonian of northern Scotland. Sediment. Geol., 19: 241–251.

Van Houten, F.B., 1974. Northern Alpine molasse and similar Cenozoic sequences of southern Europe. In: R.H. Dott Jr. and R. Shaver (Editors), Modern and Ancient Geosynclinal Sedimentation. Soc. Econ. Paleontol. Mineral. Spec. Publ., 19: 260–273.

Van Houten, F.B., 1981. The odyssey of molasse. In: A.D. Miall (Editor), Sedimentation and Tectonics in Alluvial Basins. Geol. Assoc. Can. Spec. Pap., 23: 35–48.

Walker, T.R., 1967. Formation of red beds in modern and ancient deserts. Geol. Soc. Am. Bull., 78: 353–368.

Walker, T.R., 1976. Diagenetic origin of continental red beds. In: H. Falke (Editor), The Continental Permian in Central, West, and South Europe. NATO, D. Reidel, Dordrecht, pp. 240–282.

Walker, T.R., 1984. Diagenetic albitization of potassium feldspar in arkosic sandstones. J. Sediment. Petrol., 54(1): 3–16.

Walker, T.R., Waugh, B. and Crone, A.J., 1978. Diagenesis in first-cycle desert alluvium of Cenozoic age, southwestern United States and northwestern Mexico. Geol. Soc. Am. Bull., 89: 19–32.

Wright, V.P. and Tucker, M.E., 1991. Calcretes: introduction. Int. Assoc. Sedimentol., Reprint Ser., 3: 1–22.

Zembruscki, S.G. and Chang, H.K., 1989. Gradiente geotérmico das bacias sedimentares brasileiras. Bol. Geocienc. PETROBRAS, 3(3): 215–227.

Zuffa, G.G., 1985. Optical analyses of arenites: influence of methodology on compositional results. In: G.G. Zuffa (Editor), Provenance of Arenites. NATO–ASI Ser. C, 148, D. Reidel, Dordrecht, pp. 165–189.